Exploration of the Initiation Signaling in Thoracic Aortic Aneurysm: Role of PAR1-Egr1 pathway

A Dissertation Submitted to
the Graduate School of Life and Environmental Sciences,
the University of Tsukuba
in Fulfillment of the Requirements
for the Degree of Doctor of Philosophy in Science
(Doctoral Program in Biological Sciences)

Seung Jae Shin

Table of contents

ABBREVIATIONS **2**

ABSTRACT **3**

INTRODUCTION **5**

MATERIALS & METHODS **8**

RESULTS **14**

Deletion of Egr1 prevented aneurysm formation in SMKO aorta **15**

Upregulation of Egr1, Protease Activated Receptor 1 (PAR1) and Thrombin in human TAAs **15**

PAR1 and its ligands thrombin and MMP-9, are highly activated in SMKO aortas prior to aneurysm formation **17**

PAR1 is markedly increased in SMCs during aneurysm formation in SMKO aortas . **17**

Thrombin-induced upregulation of Egr1 and Thbs1 is mediated by PAR1 ..... **18**

DISCUSSION **20**

ACKNOWLEDGEMENTS **26**

REFERNCES **28**

TABLES **37**

FIGURES & LEGENDS **45**

ABBREVIATIONS

CTRL	Control
DKO	SMKO; Egr1 knockout
EC	Endothelial cell
ECM	Extracellular matrix
Egr1	Early growth response 1
Fbln4	Fibulin-4
GAPDH	Glyceraldehyde-3-phosphate dehydrogenase
HE	Hematoxylin and eosin
HUVEC	Human umbilical endothelial cell
KD	Knockdown
MMP	Matrix metalloproteinase
p	Phosphorylation
P	Postnatal day
PAR	Protease activated receptor
SMC	Smooth muscle cell
SMKO	Smooth muscle cell-specific knockout
TAAs	Thoracic aortic aneurysms
TGF-β	transforming growth factor beta
Thbs1	Thrombospondin-1

ABSTRACT

Objective: Remodeling of the extracellular matrix (ECM) plays a vital role in cardiovascular diseases. In previous studies, a mouse model of postnatal ascending aortic aneurysms (termed *Fbln4*^{SMKO}) showed that an abnormal mechanosensing led to aneurysm formation in *Fbln4*^{SMKO} with an upregulation of the mechanosensitive transcription factor, Early growth response 1 (Egr1). However, it is still unknown whether Egr1 is essential for aneurysm development in *Fbln4*^{SMKO}, and which upstream regulators mediate the aneurysm initiation.

Approach and Results: To investigate the contribution of Egr1 in the aneurysm development, I deleted *Egr1* in *Fbln4*^{SMKO} mice and generated double knockout mice (*DKO*, *Fbln4*^{SMKO}; *Egr1*$^{-/-}$). Aneurysms were prevented in *DKO* mice (42.8%) and *Fbln4*^{SMKO}; *Egr1*$^{+/-}$ mice (26%). Ingenuity Pathway Analysis (IPA) identified Protease-activated receptor 1 (PAR1) as a potential Egr1 upstream gene. Protein and transcript levels of PAR1 were highly increased in *Fbln4*^{SMKO} aortas at postnatal day 1 before aneurysm formed, together with active thrombin and matrix metalloproteinase (MMP)-9, both of which serve as a PAR1 activator. Concordantly, protein levels of PAR1, Egr1 and thrombin were significantly increased in human thoracic aortic aneurysms. *In vitro* cyclic stretch assays (1.0 Hz, 20% strain, 8 hrs) using mouse primary vascular SMCs induced marked expression of PAR1 and secretion of prothrombin in response to mechanical stretch. Thrombin was sufficient to induce Egr1 expression in a PAR1-dependent manner.

Conclusions: I propose that mechanical stimuli activate secretion of thrombin, MMP9 in the *Fbln4*^{SMKO} aorta, then these ligands stimulate PAR1 to induce upregulation of Egr1 and initiation of ascending aortic aneurysms.

INTRODUCTION

Thoracic aortic aneurysms (TAAs) are characterized by an abnormal enlargement of the aortic lumen with silent and progressive dilatation, which may lead to dissection and/or rupture with fatal consequences. Although mortality from TAAs has been gradually declined owing to the development of technologies in medical care, the incidence increases due to associated risk factors such as hypertension and atherosclerosis that are influenced by a modern lifestyle [1]. TAAs are often associated with heritable diseases with syndromic features such as Marfan syndrome and Loeys-Dietz syndrome, which exhibit a marked activation of the transforming growth factor beta (TGF-β) signaling [2]. In addition, there are heritable TAAs without syndromic features but with underlying alterations in the contractile apparatus of vascular smooth muscle cells (SMCs) [3]. Most recently, dysfunction of mechanosensing in the aortic wall in response to hemodynamics has been proposed to be a key driver of pathogenesis of TAAs [4].

Fibulin-4 (Fbln4) is a secreted glycoprotein and a component of elastic fibers, where it is localized to microfibrils [5]. Tropoelastin is coacervated for microassembly in which Fbln4 enhances the cross-linking by lysyl oxidase (LOX), next cross-linked tropoelastin is deposited onto microfibrils, finally construct elastic fibers in vascular vessels [5,8]. Previous studies established a mouse model of postnatal TAA by deleting the fibulin-4 gene (*Fbln4*) in vascular SMCs ($Fbln4^{SMKO}$, termed *SMKO*) [6]. In *SMKO* aortas, elastic fibers fail to form normal elastic lamina-SMC connections during the early postnatal period, leading to a compensatory upregulation of mechanoresponsive molecules, such as early growth response 1 (Egr1), angiotensin-converting enzyme (ACE), thrombospondin-1 (Thbs1), and a local elevation of Ang II signaling [7,8]. Also, it is already known that serine/threonine phosphatase Ssh1 (slingshot 1) causes dephosphorylation of cofilin (active form) and disruption of actin filaments [8]. Furthermore, inhibition of Thbs1 sufficiently prevented the development of ascending aortic aneurysms and improved the integrity of elastic fibers and restored actin filaments [9]. However, the precise molecular pathways involved in the initiation of aneurysms driven by the altered mechanosensing are not fully understood.

Protease activated receptors (PARs) are prototypical member of G-protein-coupled receptors that are activated by a variety of proteases, such as thrombin, MMP family, Activated protein C (APC) and so on [10]. These ligands of protease bind to N-terminal domain of PAR1 and cleave it, and the newly unmasked N-terminus acts as a tethered ligand and trigger transmembrane signaling through G proteins or β-arrestin [10]. The

cleavage point is different depending on proteases, the cleavage site on the N-terminal PAR1 for thrombin is R_{41}-S_{42}, but the site for APC is R_{46}-N_{47} [10]. PARs are expressed on the surface of endothelium, smooth muscle cells, platelets, neutrophils, macrophages and leukemic white cells [11], and regulates platelet aggregation, cell shape, adhesion, cell proliferation, chemokine production and migration via the G-protein pathways [12]. PAR1 was identified more than 20 years ago as a thrombin receptor and three additional PARs have been identified so far: PAR2, PAR3 and PAR4 [13, 14]. PAR1 ligands are high-affinity serine proteases, including thrombin, plasmin, factor Xa and APC, known as canonical activators [15], and non-canonical activation by matrix metalloproteinases (MMPs) [16]. PAR1 also acts as a sensor for altered proteases in the extracellular microenvironment [17]. More recently, PAR1 has been shown to be critical for tissue remodeling such as angiogenesis and atherosclerosis [18, 19]. Thus, several PAR1 therapeutic antagonists have been developed to challenge application for pharmacological modulators, including F16618, E5555, and vorapaxar.

Remodeling of extracellular matrix (ECM) by matrix proteases plays a vital role in cardiovascular homeostasis. PAR1 is a member of GPCRs, activated by a variety of proteases such as thrombin, MMP-1, 2 and 9, and enables cells to respond to the extracellular environment. We have previously reported that *SMKO* mice developed ascending aortic aneurysms, and transcription factor, *Egr1*, which responds to mechanical stress, was markedly upregulated in *SMKO* aortas. It is unknown, however, why *Fbln4* loss upregulates Egr1 and Thbs1, and which intermediate receptors deliver aneurysm constitution signaling to Egr1 transcriptional factor, and finally Thbs1.

Here, I show that PAR1 is markedly upregulated in *SMKO* and human TAAs, and PAR1-mediated signals control Egr1 expression, which is causal for aneurysm development *in vivo*. Mechanistically, PAR1 and its ligands, thrombin and MMP-9, are induced by increased mechanical stress and loss of *Fbln4* as early as postnatal day (P)1 and generate abnormal microenvironment containing dysregulated protease in *SMKO* aortas. Pharmacological inhibition by thrombin inhibitor (Dabigatran) or factor Xa inhibitor (Rivaroxaban) ameliorated aneurysm phenotype in *SMKO* mice. Taken together, PAR1 upregulates the mechanoresponsive Egr1-Thbs1 pathway during aneurysm initiation. My study demonstrates the synergistic and feed-forward interactions between mechanical stress and protease activation, leading to the development of aneurysms in *SMKO* mice.

MATERIALS & METHODS

Mice. *SMKO* mice were generated previously and there were no phenotypic differences for aneurysm formation and incidence between the male and female [6]. *Egr1* null mice were purchased from The Jackson Laboratory (B6N;129-Egr1^{tm1Jmi}/J, stock number: 012924). *Fbln4*$^{+/+}$, *Fbln4*$^{lxp/+}$ or *Fbln4*$^{KO/+}$ mice containing SM22α-Cre transgene were used as control in this study. Comparisons of the phenotype were performed between animals on the same genetic background and both males and females (approximately 1:1 ratio) were used in the study. All mice were kept on a 12 hrs/12 hrs light/dark cycle under specific pathogen free condition and all animal protocols were approved by the Institutional Animal Experiment Committee of the University of Tsukuba.

Histology, immunohistochemistry and morphometric analysis. Mouse or human aortas were harvested and perfusion-fixed with 4% paraformaldehyde and embedded in paraffin. Five-micrometer sections were stained with hematoxylin and eosin (HE), Hart's (Elastic fibers) or Masson trichrome (Collagens). Images were digitally captured with Leica DM2000 microscope (Leica Microsystems, DM2000). Immunohistochemistry was done as previously described [8, 9] and morphometric analysis was performed with NIH image J software (https://imagej.nih.gov/ij/index.html) as described previously [8, 9].

Western blot analysis. Mouse or human aortas were harvested without perivascular adipose tissues. For mouse aorta, P30 thoracic aortas were divided into ascending parts (from the aortic root to the left subclavian artery) and descending parts, P1 thoracic aortas were used entirely. Aortas were minced in liquid nitrogen by pestle and dissolved in RIPA Lysis Buffer (Sigma-Aldrich, #R0278) containing 1% protease inhibitor (Sigma-Aldrich, #P8340) and 1% phosphatase inhibitor (Wako, #67-24381). The lysates were mixed with 3 x SDS sample buffer with 2-mercaptoethanol (Wako, #133-14571) and boiled at 95 °C for 5 minutes, and then were subjected to SDS-PAGE. Proteins were transferred to a PVDF membrane Immobilon®-P Transfer Membranes (Millipore, IPVH00010) and immunoblotted with indicated antibodies (provided in Table 1 and 2). Membranes were incubated with secondary antibody of anti-mouse (Bio-Rad, #170-6516, 1:1000 dilution ratio) or anti-rabbit (Bio-Rad, #170-6515, 1:1000 dilution ratio) and detected with

Chemiluminescence kit (Santa Cruz Biotechnology, #sc-2048) or SuperSignal® West Femto Maximum Sensitivity Substrate (Thermo Fisher Scientific, #RF232643).

IPA analysis. Ingenuity Pathway Analysis (IPA, QIAGEN) was carried out for searching upstream regulators. The software predicted the upstream genes of specific target through Grow Tool. I set as default for data resources, confidential level, relation types, node types and mutation and set for tissue and cell lines as endothelial cell, smooth muscle cells and cardiomyocyte and disease for cardiovascular disease, connective tissue disorders. After prediction, the predicted pathway was re-designed by PathDesigner® (Communication Infrastructure Corporation).

Human thoracic aortic tissues. The participation of patients undergoing cardiac surgery was in accordance with the research protocol approved by the Clinical Ethics Committee of University of Tsukuba Hospital (approved number #H27-217). Each patient was provided a written informed consent for the collection of aortic tissue samples. The presence of thoracic aortic aneurysm was diagnosed and documented before surgery by computed tomography. The diagnosis of thoracic aortic aneurysm was confirmed at the time of surgery by experienced cardiothoracic surgeons, and clinical phenotype diagnosis was confirmed by standard histopathology. CTRL samples were obtained from punched aortic wall tissues of patients of coronary artery disease and aortic valve stenosis.

RNA extraction and qPCR. RNA was purified from human aortas, ascending aortas of P30 mice, thoracic aortas of P1 pups, or primary SMCs and rat vascular SMCs using RNeasy® Mini Kit (QIAGEN, #74104). Five hundred ng of total RNA was subjected to reverse transcription reactions by iScript™ Reverse Transcription Supermix (Bio-Rad, #170-8841). iTaq Universal SYBR Green Supermix (Bio-Rad, #1725121) was used for amplicon detection and gene expression was normalized to the expression of housekeeping gene Glyceraldehyde 3-phosphate dehydrogenase (GAPDH). PCR reactions were carried out in triplicate in a CFX96 Real-time PCR Detection System (Bio-Rad, #1855195) with one cycle of 3 min at 95 °C, then 39 cycles of 10 sec at 95 °C and

30 sec at 55 °C. Levels of mRNA were determined using the ΔΔCt method and expressed relative to the mean ΔCt of controls. Primer sequences are provided in Table 3.

Gelatin and casein zymography. P1 CTRL and *SMKO* aortas were pulverized and homogenized in Tris buffer (10 mM Tris-HCl, pH7.4, 150 mM NaCl, 10 mM $CaCl_2$) containing 0.1% Triton-X 100. Fifteen micrograms of protein extracts were loaded on 10% gelatin or casein SDS-PAGE gels. After electrophoresis, gels were washed in 2.5% of TritonX-100 for 30 min 4 times and incubated in enzyme activating buffer at 37 °C for 72 h. After incubation, gels were rinsed with water and stained with CBB solution.

Isolation and primary culture of mouse SMCs. Primary mouse SMCs were isolated and cultured from P30 CTRL and *SMKO* ascending aortas. Ascending aortas were minced and incubated with DMEM media (Thermo Fisher Scientific, #41965039) supplemented with 20% (v/v) fetal bovine serum (FBS, Thermo Fisher Scientific, #26140079), 250 U/ml collagenase type I (Affymetrix/USB™, #AAJ13820MC) and 13.5 U/ml of elastase (Affymetrix/USB™, #15475) for 3 hrs at 37 °C with gentle shaking. Cells were pelleted and re-suspended in DMEM media containing 20% FBS, 0.1 μg/ml of rhEGF (WAKO, #05907873), 1 μg/ml of rhFGF (WAKO, #06405381) and 1 x Antibiotic-Antimycotic (Thermo Fisher Scientific, #15240062) in a 24-well dish. From the second passage, primary mouse SMCs were cultured in DMEM/F12 with 20% FBS and 1% of Antibiotic-Antimycotic.

Cell culture and thrombin. Rat vascular SMCs (Lonza, R-ASM-580, isolated from the aorta of adult male Sprague-Dawley rats) were cultured in DMEM/F12 media (Thermo Fisher Scientific, #11320033) with 20% FBS and 1% of Antibiotic-Antimycotic. Rat vascular SMCs were cultured with DMEM/F12-serum-free media for 24 hrs, then re-cultured in DMEM/F12-serum-free media with 25 Unit/mL of thrombin from bovine plasma (Sigma-Aldrich, #9002044) for indicated time points (0 hr, 0.5 hr, 1hr, 3hrs and 6 hrs). After re-culturing, cells were scraped and used for Western blot analysis.

Transfection of siRNA. Rat vascular SMCs were transiently transfected with scramble (Scr) siRNA (Thermo Fisher Scientific, #12935110), *PAR1* siRNA (*F2r* RSS303633 (Thermo Fisher Scientific, #4331182)), *Fbln4* siRNA (*Efemp2* RSS308656) and *Egr1* siRNA (*Egr1* RSS332332) by using Lipofectamine™ RNAiMAX Transfection Reagent (Thermo Fisher Scientific, #13778030). Two days after transfection, cells were used in each experiment.

Stretch assay. Cyclic stretch was performed using a uniaxial cell stretch system (Central Workshop, Tsukuba University) in the presence of 20% FBS. Four x 10^5 primary mouse SMCs were plated on a silicon chamber with Attachment Factor (Thermo Fisher Scientific, #S006100) as described previously [9, 20]. Cyclic stretch was performed with a frequency of 1.0 Hz (60 cycles / min) and an elongation of 20% for 8 hrs. After stretching, cell lysates and condition medium were harvested, condition medium was condensed by Amicon Ultra Centrifugal Filters (Millipore, # UFC200324).

Thrombin and MMP-9 activity assay. Thrombin and MMP-9 activity were measured using SensoLyte 520 Assay Kit (Anaspec, #AS-72129 for thrombin and #AS-71155 for MMP-9). Aortic tissues were excised and homogenized in assay buffer. Fifteen micrograms of protein extracts were used for the detection of active form of enzyme. Activity reactions were carried out in duplicate in Multi-label plate reader Wallac 1420 ARVOsx (PerkinElmer).

Dabigatran and Rivaroxaban treatment in vivo. *SMKO* and control pups were divided into two groups: vehicle control and inhibitor treatment. Dabigatran (30 μg/g body weight (BW); Combi-Blocks, QB-6987) or factor Xa inhibitor, Rivaroxaban (10 μg/g BW; Chemscene LLC, CS-0555) or saline was administered orally to P1 pups as described previously [21-23]. The treatments were continued from P1 to P30 every day and at P30, pups were sacrificed and the aortas were harvested for evaluation of the aneurysm phenotype.

Statistical analysis. All experiments are presented as mean ± standard error of the mean (SEM). Statistical analysis was performed using Prism 8 (Graph Pad, ver. 8.4.0). Shapiro-Wilk test was used for the normality test. When the data followed normal distribution, statistical significance was determined by either unpaired *t*-test, one-way ANOVA or two-way ANOVA followed by Tukey multiple comparison test. If the normality assumption was violated, nonparametric tests were conducted. Mann-Whitney test was used in Fig. 4C (Egr1 and Thrombin) and Fig. 8B (PAR3), Kruskal-Wallis test with Dunnett's multiple comparisons was used in Fig. 1D (total vessel area), Fig. 1E (Thbs1) and Fig. 2C (total vessel area). $P < 0.05$ denotes statistical significance.

RESULTS

Deletion of Egr1 prevented aneurysm formation in SMKO aorta

Previous studies have shown that the deletion of *Thbs1* prevents aneurysm formation in *SMKO* [9], and Egr1 is known to regulate the promotor activity of Thbs1 with the subsequent transcription and protein synthesis [24]. Egr1 is a zinc-finger transcription factor that responds to various stimuli, including mechanical stress, cell proliferation and differentiation [25, 26]. Based on these observations, I hypothesized that Egr1 contributes to the pathogenesis of aortic aneurysm in *SMKO* mice by inducing Thbs1. To test this hypothesis, I generated *SMKO* mice on an *Egr1*-null background (termed *DKO: SMKO*;*Egr1* knockout). Generation of *DKO* mice was confirmed by genotyping, and *Fbln4*$^{+/+}$;*Egr1*$^{+/+}$, *Fbln4*$^{loxp/+}$;*Egr1*$^{+/+}$, *Fbln4*$^{KO/+}$;*Egr1*$^{+/+}$ mice were used as controls (CTRL) in the following experiments (Fig. 1A). Aneurysms were examined at 1 month of age in comparison to respective CTRL littermates. Aneurysms were prevented in *DKO* mice (6 out of 14; 42.8%), but some of *DKO* still exhibited aneurysmal changes in the ascending aortas (Fig. 2A-C). Interestingly, some of *SMKO;Egr1*$^{+/-}$ mice also showed amelioration of the aneurysm (6 out of 23; 26.0%, Table 4) while none of SMKO; *Egr1*$^{+/+}$ showed improvement of the aneurysm phenotype. Histologically, elastic fibers in rescued *DKO* aortas were much organized compared to *SMKO* aortas, whereas collagen levels were comparable between *SMKO* and rescued *DKO* aortas (Fig. 1C). Morphological analysis revealed that the internal elastic lamina (IEL) perimeter and outer perimeter were smaller in *DKO* compared with *SMKO* aortas; however, wall thickness and total vessel areas remained unchanged (Fig. 1D). Thbs1 was significantly downregulated in all rescued *DKO* aortas compared to *SMKO* aortas (Fig. 1E), although some of the non-rescued *DKO* aortas showed decreased expression of Thbs1 (Fig. 2D). These data indicated that Egr1 is involved in the pathogenesis of aortic aneurysm in *SMKO* mice.

Upregulation of Egr1, Protease Activated Receptor 1 (PAR1) and Thrombin in human TAAs

To explore the upstream signaling(s) of Egr1-Thbs1, I conducted the Ingenuity pathway analysis (IPA). *F2rl3* (PAR4) [27], *Elk3* [26, 28] and *F2r* (PAR1) [27, 29] were identified as potential upstream regulators of Egr1 (Fig. 3A), especially PAR1 expression was highly increased in P90 *SMKO* aortas compared with P90 CTRL aortas (Fig. 3B). Next, to

investigate if these upstream genes are involved in the pathogenesis of human TAA, I examined transcription levels of these genes and other genes previously described to be involved in the pathogenesis of human TAA [30, 31]. TAA samples were obtained from non-syndromic sporadic patients with TAA who underwent surgery. Non-aneurysmal CTRL samples were obtained from aortic wall punch biopsies of patients undergoing coronary artery bypass surgery. There were no differences regarding sex, age, metabolic rate, blood pressure, and cardiac functions between CTRL and TAA patients (Table 5). Several genes in the angiotensin signaling pathway, vascular SMC contractile markers and synthetic markers were upregulated in TAAs compared with CTRL aortas, whereas the transcript level of *FBLN4* was decreased in TAAs (Fig. 4A). *ELK3* is a member of the ERK-regulated ternary complex factor (TCF) subfamily and acts with the transcription factor serum response factor (SRF) to activate mitogen-induced transcription [32, 33]. Interestingly, *SRF* was markedly downregulated in TAAs, whereas its target genes of vascular SMC contractile markers, including *ACTA2*, *MYH11* and *SM22α*, were upregulated in TAAs (Fig. 4A). PAR1 was also upregulated in TAAs (Fig. 4A). Since PAR1 is known to be involved in cardiovascular diseases [11, 19], I focused on PAR1 for further analyses. Consistent with the transcript levels, protein expressions of PAR1 and Egr1 were significantly increased in TAA samples compared to CTRL (Fig. 4B, C), and the cleaved form of thrombin (prethrombin and active thrombin) was also increased (Fig. 4B, C). PAR1 was negatively correlated with heart rate (Pearson r = -0.445, p = 0.010, Fig. 5) and Egr1 expression was positively correlated with heart rate (Pearson r = 0.403, p = 0.022) and systolic blood pressure (Pearson r = 0.435, p = 0.012) as shown in Fig. 6. No correlations were found between thrombin levels and clinical features (Fig. 7). Histological analysis showed that PAR1 was detected in the entire aortic wall, including intima, medial layers and adventitial layers in TAAs, and most strongly in the endothelial layer of vasa vasorum, whereas CD41, a marker for platelet, was rarely observed in the aortic wall (Fig. 4D). These data suggest that the upregulation of PAR1 in human TAAs is not predominantly due to platelet-derived PAR1. Taken together, these data demonstrated that the elevation of Egr1, PAR1 and thrombin were associated with non-syndromic sporadic TAA in humans.

PAR1 and its ligands thrombin and MMP-9, are highly activated in SMKO aortas prior to aneurysm formation

To understand the mechanistic relevance of PAR1 and Egr1 in aortic aneurysm formation, I returned to the aneurysmal mouse model (*SMKO*) and examined the expression of PAR1 in the initial stage of aortic aneurysm formation. As previous studies reported, the aortic wall began to expand in *SMKO* aortas at P7, and the aneurysm established at P30 [7]. I defined this period as a critical therapeutic time window, in which aneurysm formation can be prevented by inhibiting Ang II-mediated signaling(s) caused by local upregulation of ACE [7], and subsequent downstream signaling, Ssh1-cofilin [8]. The transcript level of *Egr1* was highly increased in *SMKO* aortas at P1, and *PAR1* was significantly increased in *SMKO* aortas among *PARs* at P1 before aneurysms formed (Fig. 8A). Western blot analysis showed a marked upregulation of PAR1, PAR3 and Egr1 in *SMKO* aortas at P1 (Fig. 8B). To investigate which PAR1 ligands are upregulated in *SMKO* aortas, I examined the ligands expression in *SMKO* aortas at P1 by qPCR (Fig. 9A). *MMP3*, *MMP8*, *MMP9* and *thrombin* were highly expressed in *SMKO* P1 aortas. Active thrombin was converted from prothrombin and prethrombin through proteolytic cleavage by factors Xa and Va (Fig. 9B). Western blot analysis showed that thrombin and prethrombin were highly increased in *SMKO* aortas at P1 (Fig. 9C), and thrombin activity was significantly increased in *SMKO* aortas compared to CTRL aortas (Fig. 9D). To identify MMP activity level, I did gelatin zymography for MMP9 (Fig. 9E). MMP9 was activated in *SMKO* aortas at P1 (Fig. 9E) and the MMP9 activity level was also highly increased in MMP9 activity assay (Fig. 9F). Next, I performed casein zymography for MMP3 and MMP8 (Fig. 9G), however, I did not detect MMP3 or MMP8. These data strongly suggest that PAR1 is activated at the initial stage of aortic aneurysm and may serve as a trigger for subsequent aneurysmal changes in *SMKO* aortas.

PAR1 is markedly increased in SMCs during aneurysm formation in SMKO aortas

To determine whether PAR1 is continuously expressed during aneurysm development, I evaluated the transcription and protein levels of *Egr1* and *PARs* in CTRL and *SMKO* aorta after aneurysms were formed. I separated thoracic aortas into ascending parts and descending parts, then performed expression analysis. Western blots showed that Egr1,

PAR1 and thrombin, but not PAR3, were upregulated in the ascending aortas of P30 *SMKO* mice (Fig. 10A). *Egr1* and *PAR1* transcripts were also upregulated in *SMKO* aortas at P90 (Fig. 11). Immunofluorescence staining revealed the thrombin expression in SMCs in addition to ECs and adventitial cells in *SMKO* aortas, indicating that thrombin was most likely derived from the vascular wall (Fig. 10B and Fig. 12). We also confirmed the upregulation of thrombin activity in P30 *SMKO* aortas (Fig. 10C). These data suggest that PAR1 was initially activated in ECs and adventitial cells, then expanded to SMCs in the ascending aorta of *SMKO* during aneurysm development. The ascending aorta is under complex mechanical stimuli due to shear stress and pulsate pressure that may contribute to the increased susceptibility to aneurysm formation [34]. In addition, SMC-specific *Fbln4* knockout mice, but not the endothelial cell-specific *Fbln4* knockout mouse developed aneurysms [6]. Therefore, I further focused on the role and regulation of PAR1 in SMCs with respect to mechanical stretch. Primary mouse SMCs isolated from CTRL and *SMKO* aortas were subjected to cyclic stretch (1.0 Hz; 20% strain) for 8hrs (Fig. 10D) or for 3, 6 and 8 hrs as shown in Fig. 13. Although PAR1 and thrombin expressions were not detected at 0, 3, 6 hrs-cyclic stretch, PAR1 was increased after 8 hrs of cyclic stretch as previously reported in human pulmonary ECs [9, 35]. Furthermore, prothrombin was markedly increased in conditioned media (CM) of CTRL and *SMKO*, but prethrombin and active thrombin were undetectable in 8 hrs cyclic stretch. These data suggest that the precursor of thrombin is produced by SMCs under mechanical stretch.

Thrombin-induced upregulation of Egr1 and Thbs1 is mediated by PAR1

To examine whether Egr1-Thbs1 is regulated by PAR1 and if deletion of *Fbln4* enhances this signaling pathway in SMCs, I performed small interfering RNA (siRNA)-mediated knockdown (KD) of *PAR1*, *Fbln4* and *Egr1* in rat vascular SMCs. Scr (as CTRL), *PAR1* or *Fbln4* or *Egr1* siRNA was administered to rat SMCs, and the efficiency of KD was confirmed by quantitative polymerase chain reaction (qPCR; Fig. 14A, Fig. 15A). I then examined the response of *PAR1*KD or *Fbln4*KD cells to thrombin in the absence of serum. In CTRL and *Fbln4*KD cells, thrombin (25 U/ml) treatment induced Egr1 expression at 1 hr and 3 hrs, and subsequently induced Thbs1 at 3 hrs and 6 hrs. In contrast, induction of Egr1 and Thbs1 by thrombin was significantly suppressed in *PAR1*KD cells (Fig. 14B). In addition, *Egr1KD* cells also reduced Thbs1 protein

expression both of at 3 hrs and 6 hrs after thrombin treatment (Fig. 15B). These data indicated that the thrombin-induced upregulation of Egr1 was mediated partly in a PAR1 dependent manner, and Thbs1 was upregulated dependent of Egr1 activation.

I finally asked if aneurysm formation can be prevented by pharmacologically inhibiting thrombin. I treated *SMKO* mice with Dabigatran (thrombin inhibitor, *n*=4) and Rivaroxaban (factor Xa inhibitor, *n*=5) from P1 to P30 and examined the formation of aneurysm at P30. Neither drug affected body weight during treatment (Fig. 16A). Dabigatran-treated (2 out of 4) and Rivaroxaban-treated (2 out of 5) *SMKO* mice showed amelioration of aneurysm phenotype (Fig. 16B). Although thrombin activity in the aortas was decreased significantly in drug-treated groups compared with untreated *SMKO*s, the levels were still higher than those of controls (Fig. 16C). Taken together, these results suggested that the increased thrombin activity may be one of the contributing factors for the aortic aneurysm initiation in *SMKO* mice.

DISCUSSION

In this study, I reported that the genetic deletion of *Egr1* negatively impacted the formation of aortic aneurysms in *SMKO* mice, and PAR1 was upstream of Egr1-Thbs1 in TAAs in *SMKO* mice. These results coincide with many of the earlier studies, thrombin and PAR1 agonist TFLLRN increased *Egr1* RNA levels and PAR1 knockout did not express *Egr1* when stimulated by thrombin and PAR1 agonist in endothelial cells [27]. Furthermore, human umbilical endothelial cells (HUVECs) increased or suppressed Thbs1 levels upon thrombin or APC stimulation, respectively [36]. PAR1 and Egr1 are both upregulated in human TAAs. In *SMKO* aortas, PAR1 was abundant and activation of thrombin and MMP-9 was evident prior to the aneurysm formation. *In vitro* analysis revealed that thrombin and mechanical stretch induced expressions of Egr1 and Thbs1 in a PAR1 dependent manner. Furthermore, the loss of *Fbln4* increases MMP-9 activity in *SMKO* aortas, all of which tips the balance for the proteolytic cleavage of PAR1 in the initiation of aortic aneurysm formation (Fig. 17).

Mechanical stress responsive factor Egr1 contributes to the aneurysm formation in SMKO aorta

Egr1 is involved in the response to stress in various organs and emerges in a variety of pathological conditions [37]. Egr1 contains a high conserved DNA-binding domain composed of zinc fingers that binds to the prototype target GC-rich consensus sequence GCG(G/T)GGGCG. I and others have shown that mechanical stretch induces Egr1 in vascular SMCs [9, 20, 25], and pressure overload upregulates Egr1 in the ascending aorta in vivo [8]. In the context of aortic aneurysms, several studies have suggested a role of Egr1 in the pathogenesis of intraluminal thrombus formation in human abdominal aortic aneurysm (AAA) [38], $CaCl_2$-induced AAA mice [39] and angiotensin II-induced AAA in apolipoprotein E-deficient mice [40]. Based on my results using *DKO* (*SMKO;Egr1*$^{-/-}$) mice in this study and genetic deletion of *Thbs1* (*SMKO;Thbs1*$^{-/-}$) in the previous study [9], I concluded that the inhibition of mechanotransduction pathway mediated by Egr1-Thbs1 was sufficient to prevent aneurysm formation in *SMKO* mice. However, the rescue efficiency of aneurysm phenotype in *SMKO;Egr1*$^{-/-}$ (42.8%) mice was lower than that of *SMKO;Thbs1*$^{-/-}$ (78.9%) mice. There are three other members of EGR family, Egr2, Egr3 and Egr4, all of which can be induced by growth factor and/or mechanical stimuli and bind to the same GC-rich consensus sequence. Indeed, I observed that *Egr2* was

upregulated in *DKO* mice (data not known), and the mechanical stretch-induced upregulation of Thbs1 was suppressed by *Egr1* KD [9] as well as *Egr2* KD, but not by *Egr3* KD (data not shown). My data is consistent with other studies showing the overlapping regulation of target genes by Egr1 and other EGRs, and a compensatory upregulation of EGR family members in the *Egr1* null mice [41, 42]. Therefore, the remaining level of Thbs1 by other EGRs in *DKO* might have supported the aneurysm formation.

Canonical activation of PAR1 by thrombin and MMP-9 in the pre-aneurysm lesions

A cleavage of the extracellular N-terminal domain of PAR1 by thrombin occurs at a canonical R_{41}-S_{42} site, which is distinct from the MMP cleavage site, resulting in conformational changes in the transmembrane domain and subsequent intracellular signal transduction [13, 16]. MMP-1 and MMP-13 cleave PAR1 at a non-canonical site, D_{39}-P_{40}, and S_{42}-F_{43}, respectively [43, 44]. On the other hand, MMP-9 has been shown to cleave conventional PAR1 site (R_{41}-S_{42}) in activated microglia [45], and I observed a marked upregulation of MMP9 activity in the P1 aortas of *SMKO* mice. In my experiments, thrombin induced Egr1 and Thbs1 via PAR1, and mechanical stretch also induced PAR1, Egr1 and Thbs1[9]. These data support the notion that mechanical signal transduction mediated by PAR1-Egr1-Thbs1 was triggered by the cleavage mediated by MMP-9 and thrombin.

Previous study showed that Thbs1 was upregulated in ECs and SMCs underneath ECs in the *SMKO* aortas [9]. Similarly, I observed thrombin expression in ECs and SMCs during aneurysm development. This observation may suggest that PAR1 propagates signals derived from ECs to SMC layers. Current study, however, failed to identify signals and a mode of signal transduction from ECs to SMCs in *SMKO* aortas. Vascular ECs can communicate with SMCs via gap junctions comprised of connexin (Cx) protein family, including Cx-37, Cx-40 and Cx-43 [46]. Interestingly, Cx-43 hemichannels are controlled by thrombin-induced cytosolic Ca^{2+} [47, 48], and Cx-43 promotor activity is regulated by PAR1 through the binding of SP-1 and AP-1 transcription factors in melanoma cells [49]. Several studies showed that Cx-43 is involved in vascular injury [50, 51]. Therefore, it will be interesting to examine the interactions between ECs and SMCs possibly mediated by PAR1 and Cx-43 in aortic aneurysms and other vascular diseases.

Loss of Fbln4 induces activation of MMP-9 in the aorta

MMPs are responsible for the degradation of the ECM in aortic aneurysms and upregulation of MMP-9 also play a crucial role in Marfan syndrome [52, 53]. I observed the activation of MMP-9 in the initial stage of aneurysm development in *SMKO* mice, as well as in the mouse model with reduced *Fbln4* expression (*Fbln4*$^{R/R}$) [7, 54]. Although *MMP-3* and *MMP-8* were upregulated at a transcriptional level in *SMKO* P1 aortas, I did not detect the activity of MMP-3 or MMP-8 in SMKO. It is possible that MT1-MMP and Plasmin, the activator of MMP-8 and MMP-3 respectively, may not be expressed in the aneurysmal wall [55, 56].

There are possible explanations for the mechanism by which *Fbln4* deficiency initiates excessive MMP-9 activation. First, TGF-β signaling has been shown to upregulate MMP-9 expression *in vivo* and *vitro* [57, 58]. TGF-β is secreted as an inactive form, then tethered onto microfibrils via latent TGF-β binding proteins [59]. Absence of *Fbln4* may affect microfibril assembly and disrupt tethering of the inactive TGF-β, increasing the bioavailability of TGF-β. MMP-9 is also known as an activator of TGF-β by proteolytic cleavage of the latent TGF-β binding proteins. Therefore, increased TGF-β signaling in *SMKO* aortas possibly induces transcription of MMP-9, in turn mediates TGF-β activation, creating a positive feed-forward loop. Second, LOX has been shown to enhance elastin synthesis and suppress MMP-9 activity [60]. LOX is a copper-dependent enzyme that catalyzes cross-linking of elastin molecules and is secreted as an inactive proenzyme, containing a N-terminal pro-peptide domain followed by the catalytic domain. The pro-peptides of the proenzyme are eventually cleaved by proteases, producing mature LOX. Since LOX activity is regulated in a Fbln4 dependent manner [61], *Fbln4* deficiency may cause inactivation of LOX and mediate an increase of the MMP-9 activity.

Less is known about the relationship between mechanical stretch and MMP-9 in aneurysm models. Recently, using a rat abdominal aortic aneurysm and dissection model, mechanical loading has been shown to induce MMP-9 expression via the stretch-activated channel[62] or via p-ERK1/2 and inflammatory mediators [63]. Cyclic stretch upregulates Nox1 NADPH oxidase and ROS in a MEF2B-dependent manner, leading to augmentation of MMP-9 activity [64]. In addition, Egr1 has also been shown to directly upregulate MMP-9 transcription in response to TNFα in non-vascular cells[65] or in collaboration with snail and SP-1 [66], in non-stretch condition. Taken together, my study

connects mechanical stress to MMP-9, which acts as a ligand for PAR1 and induces downstream signaling involving Egr1-Thbs1, which again forms a positive feed-forward loop and generates a microenvironment with dysregulated proteases.

Therapeutic potential of inhibiting PAR1 for human TAA

PAR1 inhibition might rescue the aneurysmal phenotype in *SMKO* mice. *PAR1* null mice die at around embryonic day 9-10, and exhibit vascular anomaly [67]. Therefore, the conditional knockout of PAR1 is a good design to perform rescue experiments. Besides, there are several PAR1 antagonists available to test their efficacy as an anti-aortic aneurysm drug. For example, PAR1 antagonist F16618 inhibited restenosis of rat carotid arteries after injury of balloon angioplasty [68], another antagonist E5555 also suppressed intimal thickening after balloon injury in rats [69]. Furthermore, vorapaxar is a FDA-approved PAR1-target therapeutic antagonist and currently being evaluated in large-scale clinical trials for patients with peripheral artery disease (atherosclerotic vascular disease, limb ischemia, myocardial infarct, stroke) [70]. If PAR1 antagonist efficiently blocks target receptor, it might be possible to prevent an abnormal dilatation in *SMKO* mice. The potential difficulty is that PARs form heterodimers: PAR1-PAR4, PAR1-PAR3, PAR1-PAR2, and PAR3 acts as an allosteric regulator of PAR1, enhancing the $G\alpha_{13}$ coupling [71]. Furthermore, *PAR2* deletion in cardiac fibroblasts upregulates PAR1 expressions, exhibiting a compensatory relationship among PARs [72]. In my studies, *SMKO* P1 mice highly expressed both of PAR1, PAR3, and *SMKO* P90 aortas also showed high transcription of PAR1, PAR3 in qPCR data. Thus, inhibitors or antagonists have to target both PARs effectively.

As I showed here, single administration of thrombin inhibitor (Dabigatran) or factor Xa inhibitor (Rivaroxaban) did not completely rescue aneurysm formation in *SMKO* mice, which correlated with the remaining thrombin activity. A higher dose of Dabigatran or Rivaroxaban, or combination of these drugs may be effective for prevention of aneurysms; however, it may increase risk of aortic dissection in Marfan patients, where blood clot formation was often observed [73, 74]. The potential use of PAR1 inhibitors with a combination of MMP-9 inhibitors and/or low doses of thrombin inhibitors may be effective for the prevention of aneurysm formation. It is of note that parenteral administration of factor Xa/IIa inhibitor (enoxaparin) and FXa inhibitor (fondaparinux)

effectively inhibits PAR2-, but not PAR1-, mediated Smad2/3 signaling and MMP2 expression in angiotensin II-induced aortic dilatation in *ApoE*$^{-/-}$ mice [75]. These reports provide the potential combinatorial strategies to block multiple pathways that function as the initial signal for aneurysm formation. Further investigation is necessary to establish an optimal drug protocol for TAA patients.

ACKNOWLEDGEMENTS

I thank Dr. C. Lino and Ms. M. Higashi for technical assistance. I am grateful to Ms. Huynh Thuy Hang, Mr. Tomonari Shimoda for assisting my experiment design. I am grateful to Dr. Bui Quoc Thang for preparing samples of human TAA patients. I am grateful to Honjo International scholarship for supporting my life of graduate school. I am most grateful to Professor Hiromi Yanagisawa and Assistant Professor Yoshito Yamashiro for their continuous guidance and valuable discussion through my doctoral program.

Finally, I thank all of my colleagues of the Hiromi Yanagisawa laboratory for their support in this study and my family for their support of my life in University of Tsukuba.

REFERENCES

1. Sidloff D, Choke E, Stather P, Bown M, Thompson J and Sayers R. Mortality from thoracic aortic diseases and associations with cardiovascular risk factors. *Circulation*. 2014;130:2287-94.
2. Loeys BL, Chen J, Neptune ER, Judge DP, Podowski M, Holm T, Meyers J, Leitch CC, Katsanis N, Sharifi N, Xu FL, Myers LA, Spevak PJ, Cameron DE, De Backer J, Hellemans J, Chen Y, Davis EC, Webb CL, Kress W, Coucke P, Rifkin DB, De Paepe AM and Dietz HC. A syndrome of altered cardiovascular, craniofacial, neurocognitive and skeletal development caused by mutations in TGFBR1 or TGFBR2. *Nat Genet*. 2005;37:275-81.
3. Milewicz DM, Prakash SK and Ramirez F. Therapeutics Targeting Drivers of Thoracic Aortic Aneurysms and Acute Aortic Dissections: Insights from Predisposing Genes and Mouse Models. *Annu Rev Med*. 2017;68:51-67.
4. Humphrey JD, Schwartz MA, Tellides G and Milewicz DM. Role of mechanotransduction in vascular biology: focus on thoracic aortic aneurysms and dissections. *Circ Res*. 2015;116:1448-61.
5. McLaughlin PJ, Chen Q, Horiguchi M, Starcher BC, Stanton JB, Broekelmann TJ, Marmorstein AD, McKay B, Mecham R, Nakamura T and Marmorstein LY. Targeted disruption of fibulin-4 abolishes elastogenesis and causes perinatal lethality in mice. *Mol Cell Biol*. 2006;26:1700-9.
6. Huang J, Davis EC, Chapman SL, Budatha M, Marmorstein LY, Word RA and Yanagisawa H. Fibulin-4 deficiency results in ascending aortic aneurysms: a potential link between abnormal smooth muscle cell phenotype and aneurysm progression. *Circ Res*. 2010;106:583-92.
7. Huang J, Yamashiro Y, Papke CL, Ikeda Y, Lin Y, Patel M, Inagami T, Le VP, Wagenseil JE and Yanagisawa H. Angiotensin-converting enzyme-induced activation of local angiotensin signaling is required for ascending aortic aneurysms in fibulin-4-deficient mice. *Sci Transl Med*. 2013;5:183ra58, 1-11.
8. Yamashiro Y, Papke CL, Kim J, Ringuette LJ, Zhang QJ, Liu ZP, Mirzaei H, Wagenseil JE, Davis EC and Yanagisawa H. Abnormal mechanosensing and cofilin activation promote the progression of ascending aortic aneurysms in mice. *Sci Signal*. 2015;8:ra105.
9. Yamashiro Y, Thang BQ, Shin SJ, Lino CA, Nakamura T, Kim J, Sugiyama K, Tokunaga C, Sakamoto H, Osaka M, Davis EC, Wagenseil JE, Hiramatsu Y and

Yanagisawa H. Role of Thrombospondin-1 in Mechanotransduction and Development of Thoracic Aortic Aneurysm in Mouse and Humans. *Circ Res*. 2018;123:660-672.
10. Flaumenhaft R and De Ceunynck K. Targeting PAR1: Now What? *Trends Pharmacol Sci*. 2017;38:701-716.
11. Leger AJ, Covic L and Kuliopulos A. Protease-activated receptors in cardiovascular diseases. *Circulation*. 2006;114:1070-7.
12. Macfarlane SR, Seatter MJ, Kanke T, Hunter GD and Plevin R. Proteinase-activated receptors. *Pharmacol Rev*. 2001;53:245-82.
13. Vu TK, Hung DT, Wheaton VI and Coughlin SR. Molecular cloning of a functional thrombin receptor reveals a novel proteolytic mechanism of receptor activation. *Cell*. 1991;64:1057-68.
14. Coughlin SR. Protease-activated receptors in hemostasis, thrombosis and vascular biology. *J Thromb Haemost*. 2005;3:1800-14.
15. Adams MN, Ramachandran R, Yau MK, Suen JY, Fairlie DP, Hollenberg MD and Hooper JD. Structure, function and pathophysiology of protease activated receptors. *Pharmacol Ther*. 2011;130:248-82.
16. Austin KM, Covic L and Kuliopulos A. Matrix metalloproteases and PAR1 activation. *Blood*. 2013;121:431-9.
17. Kamath L, Meydani A, Foss F and Kuliopulos A. Signaling from protease-activated receptor-1 inhibits migration and invasion of breast cancer cells. *Cancer Res*. 2001;61:5933-40.
18. Liu X, Yu J, Song S, Yue X and Li Q. Protease-activated receptor-1 (PAR-1): a promising molecular target for cancer. *Oncotarget*. 2017;8:107334-107345.
19. Jaberi N, Soleimani A, Pashirzad M, Abdeahad H, Mohammadi F, Khoshakhlagh M, Khazaei M, Ferns GA, Avan A and Hassanian SM. Role of thrombin in the pathogenesis of atherosclerosis. *J Cell Biochem*. 2019;120:4757-4765.
20. Yamashiro Y, Thang BQ, Ramirez K, Shin SJ, Kohata T, Ohata S, Nguyen TAV, Ohtsuki S, Nagayama K and Yanagisawa H. Matrix mechanotransduction mediated by thrombospondin-1/integrin/YAP in the vascular remodeling. *Proc Natl Acad Sci U S A*. 2020;117:9896-9905.
21. DeFeo K, Hayes C, Chernick M, Ryn JV and Gilmour SK. Use of dabigatran etexilate to reduce breast cancer progression. *Cancer Biol Ther*. 2010;10:1001-8.

22. Kondo H, Abe I, Fukui A, Saito S, Miyoshi M, Aoki K, Shinohara T, Teshima Y, Yufu K and Takahashi N. Possible role of rivaroxaban in attenuating pressure-overload-induced atrial fibrosis and fibrillation. *J Cardiol*. 2018;71:310-319.
23. Terry CM, He Y and Cheung AK. Rivaroxaban improves patency and decreases inflammation in a mouse model of catheter thrombosis. *Thromb Res*. 2016;144:106-12.
24. Zhao HY, Ooyama A, Yamamoto M, Ikeda R, Haraguchi M, Tabata S, Furukawa T, Che XF, Zhang S, Oka T, Fukushima M, Nakagawa M, Ono M, Kuwano M and Akiyama S. Molecular basis for the induction of an angiogenesis inhibitor, thrombospondin-1, by 5-fluorouracil. *Cancer Res*. 2008;68:7035-41.
25. Morawietz H, Ma YH, Vives F, Wilson E, Sukhatme VP, Holtz J and Ives HE. Rapid induction and translocation of Egr-1 in response to mechanical strain in vascular smooth muscle cells. *Circ Res*. 1999;84:678-87.
26. Gross C, Buchwalter G, Dubois-Pot H, Cler E, Zheng H and Wasylyk B. The ternary complex factor net is downregulated by hypoxia and regulates hypoxia-responsive genes. *Mol Cell Biol*. 2007;27:4133-41.
27. Kataoka H, Hamilton JR, McKemy DD, Camerer E, Zheng YW, Cheng A, Griffin C and Coughlin SR. Protease-activated receptors 1 and 4 mediate thrombin signaling in endothelial cells. *Blood*. 2003;102:3224-31.
28. Ayadi A, Zheng H, Sobieszczuk P, Buchwalter G, Moerman P, Alitalo K and Wasylyk B. Net-targeted mutant mice develop a vascular phenotype and up-regulate egr-1. *EMBO J*. 2001;20:5139-52.
29. Waitkus MS, Chandrasekharan UM, Willard B, Haque SJ and DiCorleto PE. STAT3-mediated coincidence detection regulates noncanonical immediate early gene induction. *J Biol Chem*. 2013;288:11988-2003.
30. Lino Cardenas CL, Kessinger CW, MacDonald C, Jassar AS, Isselbacher EM, Jaffer FA and Lindsay ME. Inhibition of the methyltranferase EZH2 improves aortic performance in experimental thoracic aortic aneurysm. *JCI Insight*. 2018;3.
31. Liu R, Lo L, Lay AJ, Zhao Y, Ting KK, Robertson EN, Sherrah AG, Jarrah S, Li H, Zhou Z, Hambly BD, Richmond DR, Jeremy RW, Bannon PG, Vadas MA and Gamble JR. ARHGAP18 Protects Against Thoracic Aortic Aneurysm Formation by Mitigating the Synthetic and Proinflammatory Smooth Muscle Cell Phenotype. *Circ Res*. 2017;121:512-524.

32. Nozaki M, Onishi Y, Kanno N, Ono Y and Fujimura Y. Molecular cloning of Elk-3, a new member of the Ets family expressed during mouse embryogenesis and analysis of its transcriptional repression activity. *DNA Cell Biol*. 1996;15:855-62.
33. Gualdrini F, Esnault C, Horswell S, Stewart A, Matthews N and Treisman R. SRF Co-factors Control the Balance between Cell Proliferation and Contractility. *Mol Cell*. 2016;64:1048-1061.
34. Wagenseil JE. Bio-chemo-mechanics of thoracic aortic aneurysms. *Curr Opin Biomed Eng*. 2018;5:50-57.
35. Birukova AA, Arce FT, Moldobaeva N, Dudek SM, Garcia JG, Lal R and Birukov KG. Endothelial permeability is controlled by spatially defined cytoskeletal mechanics: atomic force microscopy force mapping of pulmonary endothelial monolayer. *Nanomedicine*. 2009;5:30-41.
36. Riewald M and Ruf W. Protease-activated receptor-1 signaling by activated protein C in cytokine-perturbed endothelial cells is distinct from thrombin signaling. *J Biol Chem*. 2005;280:19808-14.
37. Khachigian LM. Early growth response-1 in the pathogenesis of cardiovascular disease. *J Mol Med (Berl)*. 2016;94:747-53.
38. Shin IS, Kim JM, Kim KL, Jang SY, Jeon ES, Choi SH, Kim DK, Suh W and Kim YW. Early growth response factor-1 is associated with intraluminal thrombus formation in human abdominal aortic aneurysm. *J Am Coll Cardiol*. 2009;53:792-9.
39. Charolidi N, Pirianov G, Torsney E, Pearce S, Laing K, Nohturfft A and Cockerill GW. Pioglitazone Identifies a New Target for Aneurysm Treatment: Role of Egr1 in an Experimental Murine Model of Aortic Aneurysm. *J Vasc Res*. 2015;52:81-93.
40. Martin-McNulty B, Tham DM, da Cunha V, Ho JJ, Wilson DW, Rutledge JC, Deng GG, Vergona R, Sullivan ME and Wang YX. 17 Beta-estradiol attenuates development of angiotensin II-induced aortic abdominal aneurysm in apolipoprotein E-deficient mice. *Arterioscler Thromb Vasc Biol*. 2003;23:1627-32.
41. Gokey NG, Lopez-Anido C, Gillian-Daniel AL and Svaren J. Early growth response 1 (Egr1) regulates cholesterol biosynthetic gene expression. *J Biol Chem*. 2011;286:29501-10.

42. Kumbrink J, Kirsch KH and Johnson JP. EGR1, EGR2, and EGR3 activate the expression of their coregulator NAB2 establishing a negative feedback loop in cells of neuroectodermal and epithelial origin. *J Cell Biochem*. 2010;111:207-17.
43. Trivedi V, Boire A, Tchernychev B, Kaneider NC, Leger AJ, O'Callaghan K, Covic L and Kuliopulos A. Platelet matrix metalloprotease-1 mediates thrombogenesis by activating PAR1 at a cryptic ligand site. *Cell*. 2009;137:332-43.
44. Jaffre F, Friedman AE, Hu Z, Mackman N and Blaxall BC. beta-adrenergic receptor stimulation transactivates protease-activated receptor 1 via matrix metalloproteinase 13 in cardiac cells. *Circulation*. 2012;125:2993-3003.
45. Lee EJ, Woo MS, Moon PG, Baek MC, Choi IY, Kim WK, Junn E and Kim HS. Alpha-synuclein activates microglia by inducing the expressions of matrix metalloproteinases and the subsequent activation of protease-activated receptor-1. *J Immunol*. 2010;185:615-23.
46. Okamoto T and Suzuki K. The Role of Gap Junction-Mediated Endothelial Cell-Cell Interaction in the Crosstalk between Inflammation and Blood Coagulation. *Int J Mol Sci*. 2017;18.
47. Sacks RS, Firth AL, Remillard CV, Agange N, Yau J, Ko EA and Yuan JX. Thrombin-mediated increases in cytosolic [Ca2+] involve different mechanisms in human pulmonary artery smooth muscle and endothelial cells. *Am J Physiol Lung Cell Mol Physiol*. 2008;295:L1048-55.
48. De Bock M, Wang N, Bol M, Decrock E, Ponsaerts R, Bultynck G, Dupont G and Leybaert L. Connexin 43 hemichannels contribute to cytoplasmic Ca2+ oscillations by providing a bimodal Ca2+-dependent Ca2+ entry pathway. *J Biol Chem*. 2012;287:12250-66.
49. Villares GJ, Dobroff AS, Wang H, Zigler M, Melnikova VO, Huang L and Bar-Eli M. Overexpression of protease-activated receptor-1 contributes to melanoma metastasis via regulation of connexin 43. *Cancer Res*. 2009;69:6730-7.
50. Liao Y, Regan CP, Manabe I, Owens GK, Day KH, Damon DN and Duling BR. Smooth muscle-targeted knockout of connexin43 enhances neointimal formation in response to vascular injury. *Arterioscler Thromb Vasc Biol*. 2007;27:1037-42.
51. Han XJ, He D, Xu LJ, Chen M, Wang YQ, Feng JG, Wei MJ, Hong T and Jiang LP. Knockdown of connexin 43 attenuates balloon injury-induced vascular

restenosis through the inhibition of the proliferation and migration of vascular smooth muscle cells. *Int J Mol Med*. 2015;36:1361-8.

52. Longo GM, Xiong W, Greiner TC, Zhao Y, Fiotti N and Baxter BT. Matrix metalloproteinases 2 and 9 work in concert to produce aortic aneurysms. *J Clin Invest*. 2002;110:625-32.

53. Segura AM, Luna RE, Horiba K, Stetler-Stevenson WG, McAllister HA, Jr., Willerson JT and Ferrans VJ. Immunohistochemistry of matrix metalloproteinases and their inhibitors in thoracic aortic aneurysms and aortic valves of patients with Marfan's syndrome. *Circulation*. 1998;98:II331-7; discussion II337-8.

54. Kaijzel EL, van Heijningen PM, Wielopolski PA, Vermeij M, Koning GA, van Cappellen WA, Que I, Chan A, Dijkstra J, Ramnath NW, Hawinkels LJ, Bernsen MR, Lowik CW and Essers J. Multimodality imaging reveals a gradual increase in matrix metalloproteinase activity at aneurysmal lesions in live fibulin-4 mice. *Circ Cardiovasc Imaging*. 2010;3:567-77.

55. Holopainen JM, Moilanen JA, Sorsa T, Kivela-Rajamaki M, Tervahartiala T, Vesaluoma MH and Tervo TM. Activation of matrix metalloproteinase-8 by membrane type 1-MMP and their expression in human tears after photorefractive keratectomy. *Invest Ophthalmol Vis Sci*. 2003;44:2550-6.

56. Allaire E, Hasenstab D, Kenagy RD, Starcher B, Clowes MM and Clowes AW. Prevention of aneurysm development and rupture by local overexpression of plasminogen activator inhibitor-1. *Circulation*. 1998;98:249-55.

57. Kim ES, Kim MS and Moon A. TGF-beta-induced upregulation of MMP-2 and MMP-9 depends on p38 MAPK, but not ERK signaling in MCF10A human breast epithelial cells. *Int J Oncol*. 2004;25:1375-82.

58. Stuelten CH, DaCosta Byfield S, Arany PR, Karpova TS, Stetler-Stevenson WG and Roberts AB. Breast cancer cells induce stromal fibroblasts to express MMP-9 via secretion of TNF-alpha and TGF-beta. *J Cell Sci*. 2005;118:2143-53.

59. Isogai Z, Ono RN, Ushiro S, Keene DR, Chen Y, Mazzieri R, Charbonneau NL, Reinhardt DP, Rifkin DB and Sakai LY. Latent transforming growth factor beta-binding protein 1 interacts with fibrillin and is a microfibril-associated protein. *J Biol Chem*. 2003;278:2750-7.

60. Kothapalli CR and Ramamurthi A. Lysyl oxidase enhances elastin synthesis and matrix formation by vascular smooth muscle cells. *J Tissue Eng Regen Med*. 2009;3:655-61.
61. Horiguchi M, Inoue T, Ohbayashi T, Hirai M, Noda K, Marmorstein LY, Yabe D, Takagi K, Akama TO, Kita T, Kimura T and Nakamura T. Fibulin-4 conducts proper elastogenesis via interaction with cross-linking enzyme lysyl oxidase. *Proc Natl Acad Sci U S A*. 2009;106:19029-34.
62. Qiu Z, Chen L, Cao H, Chen Q and Peng H. Mechanical Strain Induced Expression of Matrix Metalloproteinase-9 via Stretch-Activated Channels in Rat Abdominal Aortic Dissection. *Med Sci Monit*. 2017;23:1268-1276.
63. Hu Y, Lu L, Qiu Z, Huang Q, Chen Y and Chen L. Mechanical stretch aggravates aortic dissection by regulating MAPK pathway and the expression of MMP-9 and inflammation factors. *Biomed Pharmacother*. 2018;108:1294-1302.
64. Rodriguez AI, Csanyi G, Ranayhossaini DJ, Feck DM, Blose KJ, Assatourian L, Vorp DA and Pagano PJ. MEF2B-Nox1 signaling is critical for stretch-induced phenotypic modulation of vascular smooth muscle cells. *Arterioscler Thromb Vasc Biol*. 2015;35:430-8.
65. Shin SY, Kim JH, Baker A, Lim Y and Lee YH. Transcription factor Egr-1 is essential for maximal matrix metalloproteinase-9 transcription by tumor necrosis factor alpha. *Mol Cancer Res*. 2010;8:507-19.
66. Wu WS, You RI, Cheng CC, Lee MC, Lin TY and Hu CT. Snail collaborates with EGR-1 and SP-1 to directly activate transcription of MMP 9 and ZEB1. *Sci Rep*. 2017;7:17753.
67. Connolly AJ, Ishihara H, Kahn ML, Farese RV, Jr. and Coughlin SR. Role of the thrombin receptor in development and evidence for a second receptor. *Nature*. 1996;381:516-9.
68. Chieng-Yane P, Bocquet A, Letienne R, Bourbon T, Sablayrolles S, Perez M, Hatem SN, Lompre AM, Le Grand B and David-Dufilho M. Protease-activated receptor-1 antagonist F 16618 reduces arterial restenosis by down-regulation of tumor necrosis factor alpha and matrix metalloproteinase 7 expression, migration, and proliferation of vascular smooth muscle cells. *J Pharmacol Exp Ther*. 2011;336:643-51.
69. Kogushi M, Matsuoka T, Kuramochi H, Murakami K, Kawata T, Kimura A, Chiba K, Musha T, Suzuki S, Kawahara T, Kajiwara A and Hishinuma I. Oral

administration of the thrombin receptor antagonist E5555 (atopaxar) attenuates intimal thickening following balloon injury in rats. *Eur J Pharmacol*. 2011;666:158-64.

70. Bonaca MP, Scirica BM, Creager MA, Olin J, Bounameaux H, Dellborg M, Lamp JM, Murphy SA, Braunwald E and Morrow DA. Vorapaxar in patients with peripheral artery disease: results from TRA2{degrees}P-TIMI 50. *Circulation*. 2013;127:1522-9, 1529e1-6.

71. Nieman MT. Protease-activated receptors in hemostasis. *Blood*. 2016;128:169-77.

72. Friebel J, Weithauser A, Witkowski M, Rauch BH, Savvatis K, Dorner A, Tabaraie T, Kasner M, Moos V, Bosel D, Gotthardt M, Radke MH, Wegner M, Bobbert P, Lassner D, Tschope C, Schutheiss HP, Felix SB, Landmesser U and Rauch U. Protease-activated receptor 2 deficiency mediates cardiac fibrosis and diastolic dysfunction. *Eur Heart J*. 2019;40:3318-3332.

73. Kantelhardt SR, Pasnoori V, Varma J, Rezazadeh A and Dawn B. Recurrent aortic dissection in Marfan's syndrome: possible effects of anticoagulation. *Cardiol Rev*. 2003;11:240-3.

74. Dean JC. Marfan syndrome: clinical diagnosis and management. *Eur J Hum Genet*. 2007;15:724-33.

75. Moran CS, Seto SW, Krishna SM, Sharma S, Jose RJ, Biros E, Wang Y, Morton SK and Golledge J. Parenteral administration of factor Xa/IIa inhibitors limits experimental aortic aneurysm and atherosclerosis. *Sci Rep*. 2017;7:43079.

12

TABLES

Table 1. Information for antibodies

Antibody	Source	Catalog number
THBS1	Neomarkers	#MS-421
Thrombin R (ATAP2)	Santa Cruz Biotechnology	#sc-13503
PAR1	Novus Biologicals	#NBP1-71770
PAR3	Santa Cruz Biotechnology	#sc-393127
PAR4	Allomone labs	#APR-034
EGR1	Cell Signaling	#4154
GAPDH	Cell Signaling	#2118
Thrombin	Santa Cruz Biotechnology	#sc-271449
CD41	Abcam	#ab134131
Ms IgG Isotype Control	Invitrogen	#10400C

Table 2. Major Resources Table of antibodies

Western blotting

Target antigen	Vendor or Source	Catalog #	Working concentration	Lot # (preferred but not required)
THBS1	Neomarkers	#MS-421	400 ng/mL	421P1708D
PAR1	Novus Biologicals	#NBP1-71770	2 µg/mL	A3
PAR3	Santa Cruz Biotechnology	#sc-393127	400 ng/mL	K0818
PAR4	Allomone labs	#APR-034	4 µg/mL	AN-01
EGR1	Cell Signaling	#4154	1:500	3
GAPDH	Cell Signaling	#2118	1:1000	10
Thrombin	Santa Cruz Biotechnology	#sc-271449	400 ng/mL	G0317

Immunofluorescence and immunohistochemistry

Target antigen	Vendor or Source	Catalog #	Working concentration	Lot # (preferred but not required)
Thrombin R (ATAP2)	Santa Cruz Biotechnology	#sc-13503	4 µg/mL	D1417
Thrombin	Santa Cruz Biotechnology	#sc-271449	1 µg/mL	G0317
CD41	Abcam	#ab134131	7.21 µg/mL	GR3259786-4
Ms IgG Isotype Control	invitrogen	#10400C	1-4 µg/mL	TH274695

Table 3. Information for qPCR primers

Human genes

Gene	Sequence
ACE	F: 5'-TGGTGACTGATGAGGCTGAG-3'
	R: 5'-TCTTGCTGGTCTCTGTGGTG -3'
ANG	F: 5'- GCCTCCTCGCCAATGATTCCA -3'
	R: 5'- CGTCCTGTCACTCGCTGCTG -3'
ENPEP	F: 5'-TGACACCGTTCACGTTAAGCA -3'
	R: 5'-GGAAGAGGCAAGTAGGCTACCA -3'
REN	F: 5'- GAAAGCCTGAAGGAACGA -3'
	R: 5'- GTACTGGGTGTCCATGTAGTT -3'
ACTA2	F: 5'- AAAAGACAGCTACGTGGGTGA -3'
	R: 5'- GCCATGTTCTATCGGGTACTTC -3'
MYH11	F: 5'- CGCCAAGAGACTCGTCTGG -3'
	R: 5'- TCTTTCCCAACCGTGACCTTC -3'
MYOCD	F: 5'- TTTCAGAGGTAACACAGCCTCCATCC -3'
	R: 5'- ACTGTCGGTGGCATAGGGATCAAA -3'
***TAGLN* (*SM22α*)**	F: 5'-AGTGCAGTCCAAAATCGAGAAG-3'
	R: 5'-CTTGCTCAGAATCACGCCAT-3'
SRF	F: 5'- ACTGCCTTCAGTAGGAACAA -3'
	R: 5'- TTCAAGCACACACACTCACT -3'
TGFB1	F: 5'- GCGTGCTAATGGTGGAAAC -3'
	R: 5'- CGGTGACATCAAAAGATAACCAC -3'
TGFB2	F: 5'- CAGCACACTCGATATGGACCA -3'
	R: 5'- CCTCGGGCTCAGGATAGTCT -3'
TGFB3	F: 5'- GATGATTCCCCCACACCG -3'
	R: 5'- CTGCACTGCGGAGGTATG -3'
CTGF	F: 5'-TTGGCCCAGACCCAACTATG-3'
	R: 5'-CAGGAGGCGTTGTCATTGGT-3'
PAI1	F: 5'-TGCTGGTGAATGCCCTCTACT-3'
	R: 5'-CGGTCATTCCCAGGTTCTCTA-3'
MMP2	F: 5'- TCCGTGTGAAGTATGGGAAC -3'

	R: 5’- TGGGGACAGAAGCCG -3’
MMP3	F: 5’- AGTCTTCCAATCCTACTGTTGCT -3’
	R: 5’- TCCCCGTCACCTCCAATCC -3’
COL1A1	F: 5’- GAGGGCCAAGACGAAGACATC -3’
	R: 5’- CAGATCACGTCATCGCACAAC -3’
COL3A1	F: 5’- GGAGCTGGCTACTTCTCGC -3’
	R: 5’- GGGAACATCCTCCTTCAACAG -3’
ELK3	F: 5’-AGTCCACTGCTCTCCAGCAT-3’
	R: 5’-GCAGACGTCATCAGGATTT-3’
***F2R* (*PAR1*)**	F: 5’-ACCCTGCTCGAAGGCTACTA-3’
	R: 5’-GTGGAAATGATCAGCGGCAC-3’
***F2RL3* (*PAR4*)**	F: 5’-CTGCGTGGATCCCTTCATCT-3’
	R: 5’-CCTGCCCGCACCTTGTC-3’
EGR1	F: 5’-CAGCACCTTCAACCCTCAG-3’
	R: 5’-CACAAGGTGTTGCCACTGTT-3’
GAPDH	F: 5’- CGTGGAAGGACTCATGACCA -3’
	R: 5’- GGCAGGGATGATGTTCTGGA -3’
FBLN4	F: 5’-TTGATGTGAACGAGTGTGACATGG-3’
	R: 5’-CAGAGGTAGCTGGAGTAGCTACAC-3’

Mouse genes

Gene	Sequence
Gapdh	F: 5’-TGACGTGCCGCCTGGAGAAA-3’
	R: 5’-AGTGTAGCCCAAGATGCCCTTCAG-3’
Fbln4	F: 5’-GCACTGCCGGGATGTCA-3’
	R: 5’-GCATTTCATCTCACCCTTGCA-3’
Egr1	F: 5’-CGAGCGAACAACCCTATGAG-3’
	R: 5’-CATTATTCAGAGCGATGTCAGAAA-3’
***F2r* (PAR1)**	F: 5’-CCTATGAGCCAGCCAGAATC-3’
	R: 5’-TAGACTGCCCTACCCTCCAG-3’
***F2rl1* (PAR2)**	F: 5’-TCTCTGCACCAATCACAAGC-3’

	R: 5’-CTTAGCCTTCTTGCCAGGTG-3’
***F2rl2* (PAR3)**	F: 5’-TTCTGCCAGTCACTGTTTGC-3’
	R: 5’-CGGGACACTCCGCTTTTAT-3’
***F2rl3* (PAR4)**	F: 5’-TGCTGTATCCTTTGGTGCTG-3’
	R: 5’-CCTCGTGGATTAGGCTTGTC-3’
Elk3a	F: 5’-TGTGTTCGGCCCTTGCA-3’
	R: 5’-TGTGTTCGGCCCTGCA-3’
Elk3b	F: 5’-CCTTCTTCACCGCACAGACA-3’
	R: 5’-TGTGTTCGGCCCTGCA-3’
Elk3c	F: 5’-TCAGGACTGTGATCAGACACCAA-3’
	R: 5’-TGTGTTCGGCCCTGCA-3’
Elk3d	5’-CTGAGATACTATTACGACAAGACACCAA-3’
	R: 5’-TGTGTTCGGCCCTGCA-3’
MMP1	F: 5’-AACTACATTTAGGGGAGAGGTGT-3’
	R: 5’-GCAGCGTCAAGTTTAACTGGAA-3’
MMP2	F: 5’-CAAGTTCCCCGGCGAGTC-3’
	R: 5’-TTCTGGTCAAGGTCACCTGTC-3’
MMP3	F: 5’-ACATGGAGACTTTGTCCCTTTTG-3’
	R: 5’-TTGGCTGAGTGGTAGAGTCCC-3’
MMP8	F: 5’-AACCAGGCCAAGGTATTGGA-3’
	R: 5’-TTCATGAGCAGCCACGAGAA-3’
MMP9	F: 5’-CTGGACAGCCAGACACTAAAG-3’
	R: 5’-CTCGCGGCAAGTCTTCAGAG-3’
Thrombin	F: 5’-CCGAAAGGGCAACCTAGAGC-3’
	R: 5’-GGCCCAGAACACGTCTGTG-3’

Rat genes

Gene	Sequence
Gapdh	F: 5’-AATGTATCCGTTGTGGATCTGAC-3’
	R: 5’-TCTCTTGCTCTCAGTATCCTTGC-3’
***F2r* (PAR1)**	F: 5’-AGCCTTCCCCTGAACATCCT-3’
	R: 5’-ACGGCCGGCTTCTTGAC-3’

Fbln4	F: 5'-CACACAGGGGGACTTCTACATTA-3'
	R: 5'-CCTTCTTTCTCCCTTTATTGTCC-3'
Egr1	F: 5'-ACATCGCTCTGAATAACGAGAAG-3'
	R: 5'-ATGTCAGTGTTGGGAGTAGGAAA-3'

Table 4. Summary of aneurysm phenotype in *SMKO* mice with *Egr1* deficiency.

Genotype	Phenotype			
	Aneurysm	Dilatation or normal	Total number (rescue ratio)	p-value
SMKO;EGR1$^{-/-}$ (DKO)	**8**	**6**	**14 (42.8 %)**	**0.017 ***
SMKO; EGR1$^{+/-}$	**17**	**6**	**23 (26.0 %)**	**0.07**
SMKO; EGR1$^{+/+}$ (SMKO)	**11**	**0**	**11 (0 %)**	

* $P < 0.05$, Fisher's exact *t*-test (compare to *SMKO* group).

Table 5. Characterization of CTRL and TAA patients.

	CTRL (9 Patients)	TAA (32 Patients)	*p*- Value (*t*-Test)
Male (%)	55.5	62.5	
Median of age (mini – max; years-old)	72 (53-83)	66 (47-79)	0.102
Body mass index (BMI; kg/m^2)	22.30 ± 3.22	22.81 ± 3.22	0.69
Heart rate (HR; bpm)	71.77 ± 9.53	72.58 ± 12.29	0.858
Systolic blood pressure (SBP; mmHg)	129.88 ± 17.62	131.12 ± 19.81	0.87
Aortic diameter (mm)	36.33 ± 6.15	53.85 ± 7.84	*** P <0.001
Ejection fraction (EF; %)	60.11 ± 15.74	59.80 ± 12.20	0.95
Internal ventricular septum (IVS; mm)	10.74 ± 2.60	10.80 ± 1.82	0.922
left ventricular posterior wall (LVPW; mm))	10.66 ± 2.40	10.58 ± 1.76	0.92

***$P < 0.001$, unpaired *t*-test.

FIGURES & LEGENDS

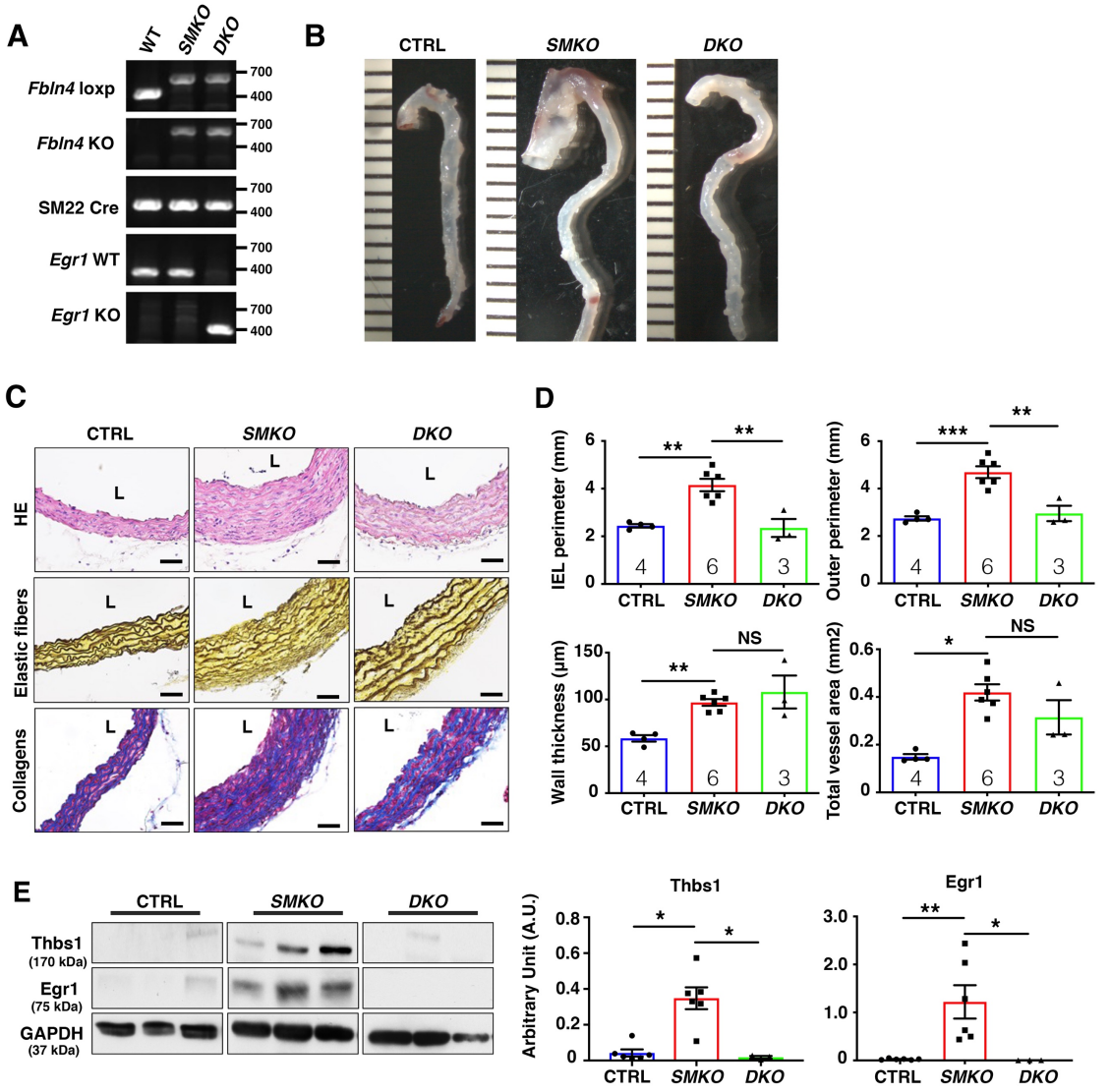

Figure 1. Deletion of *Egr1* attenuates aneurysm formation in *SMKO* mice.

(A) Genomic PCR confirming the genotype of *SMKO* and *Egr1* mutants. *Fbln4* (F4) loxp: 670 bp, WT; 470 bp, *F4* KO; 540 bp, *SM22α*-Cre; 500 bp, *Egr1* WT; 414, *Egr1* KO; 420 bp. **(B)** Gross photos of CTRL, *SMKO*, and *SMKO;Egr1*$^{-/-}$ (*DKO*) aortas at postnatal day (P) 30. Scale of bars is 1 mm. **(C)** Histological images of cross sections of the ascending aortas from P30 CTRL (n=4), *SMKO* (n=6) and *DKO* (n=3) stained with hematoxylin and eosin (HE), Hart's (Elastic fibers) and Masson's trichrome (Collagens). L: lumen. Scale bars are 40 μm. **(D)** Morphometric analysis showing internal elastic lamellar (IEL) perimeter, outer perimeter, wall thickness, and total vessel area. Bars are means ± SEM. $^{**}P < 0.01$. $^{***}P < 0.001$, one-way ANOVA for IEL perimeter, outer perimeter and wall thickness and Kruskal-Wallis test for total vessel area. NS: not significant. Number of

animals are indicated in each bar. **(E)** Western blots of Thbs1, Egr1 and GAPDH in the ascending aortas from P30 CTRL (*n*=6), *SMKO* (*n*=6) and *DKO* (*n*=3). Quantification graphs are shown on the right. * $P < 0.05$, ** $P < 0.01$, one-way ANOVA for Egr1, Kruskal-Wallis test for Thbs1.

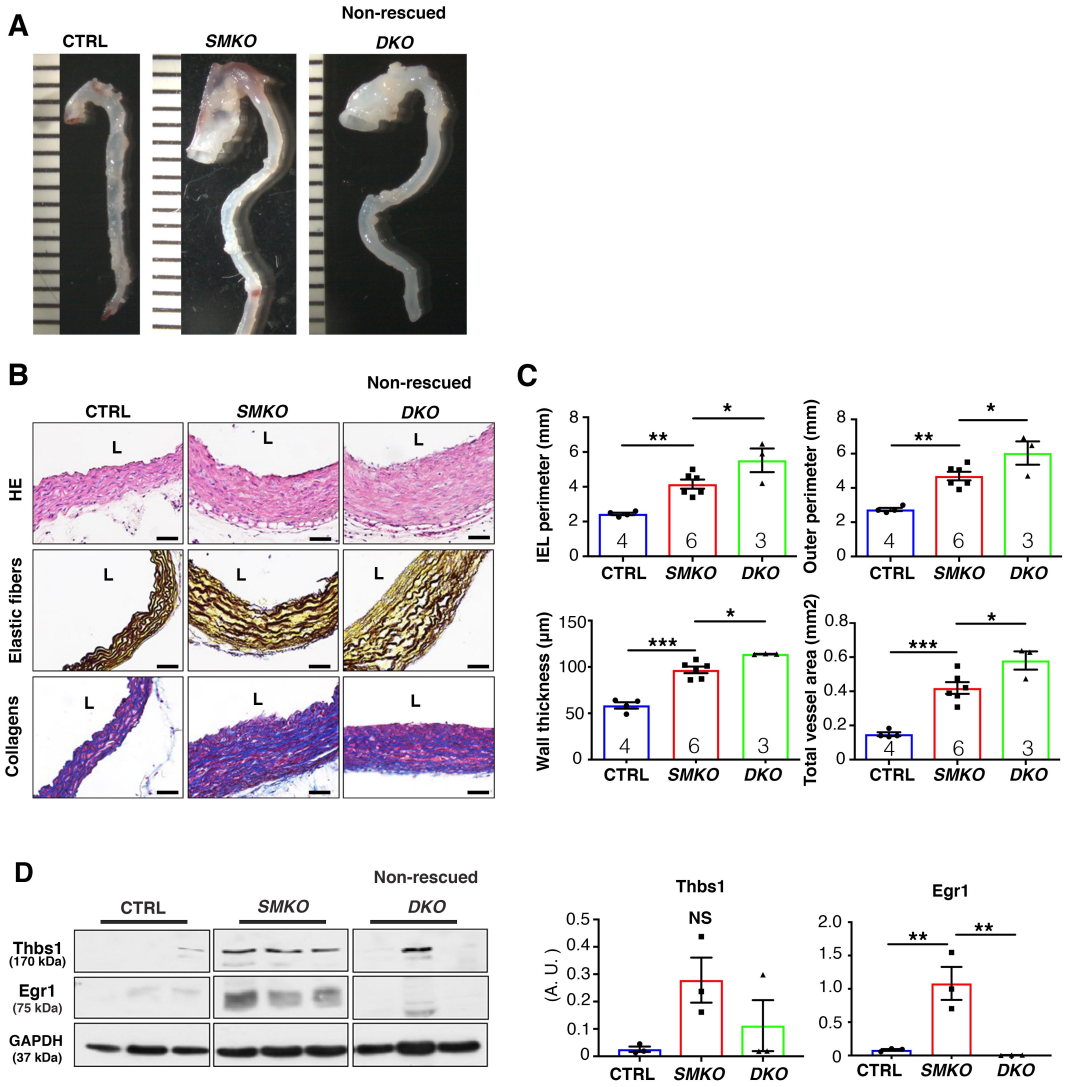

Figure 2. Evaluation of non-rescued *DKO* mice for aneurysm formation.

(A) Gross photos of CTRL, *SMKO*, and non-rescued *DKO* aortas at P30. Scale of bars is 1 mm. **(B)** Histological images of cross sections of the ascending aortas from P30 CTRL (*n*=4), *SMKO* (*n*=6) and non-rescued *DKO* (*n*=3) stained with hematoxylin and eosin (HE), Hart's (Elastic fibers) and Masson's trichrome (Collagens). L: lumen. Scale bars are 40 μm. **(C)** Morphometric analysis showing IEL perimeter, outer perimeter, wall thickness, and total vessel area. Bars are means ± SEM. **P* < 0.05, ***P* < 0.01, and ****P* < 0.001, one-way ANOVA for IEL perimeter, outer perimeter and wall thickness and Kruskal-Wallis test for total vessel area. Number of animals are indicated in each bar. **(D)** Western blots of Thbs1, Egr1 and GAPDH in the ascending aortas from P30 CTRL (*n*=3), *SMKO* (*n*=3) and non-rescued *DKO* (*n*=3). Quantification graphs are

shown on the right. ** $P < 0.01$, one-way ANOVA for Egr1 and Kruskal-Wallis test for Thbs1. NS: not significant.

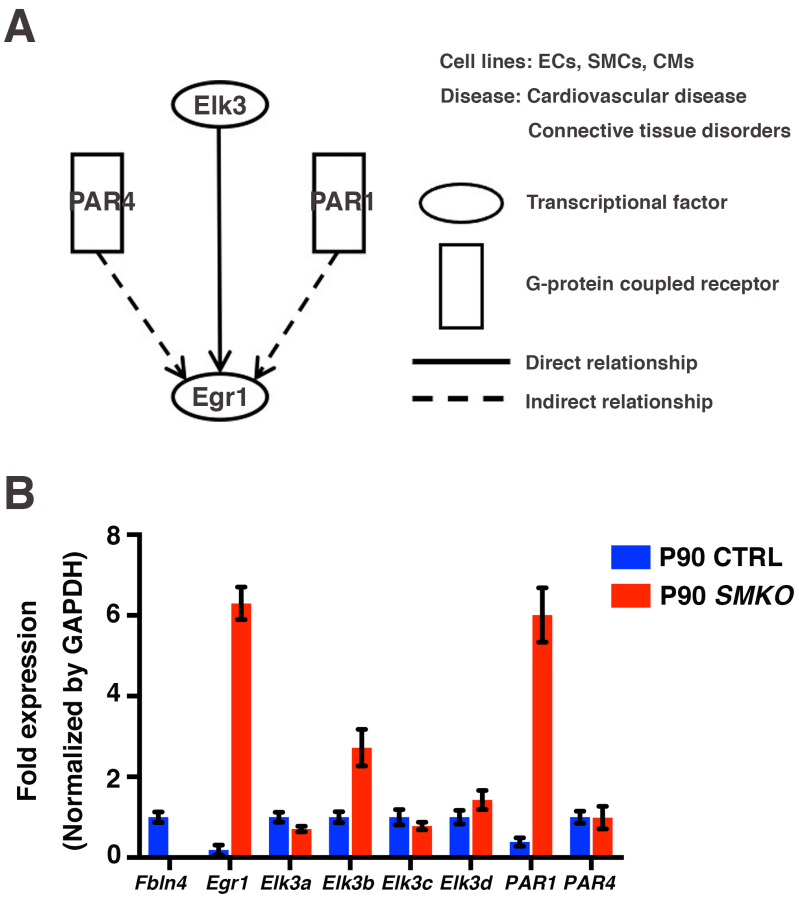

Figure 3. PAR1, PAR4 and Elk3 are identified as a possible upstream regulator of *Egr1*. (A) Bioinformatic analysis using Ingenuity Pathway Analysis (IPA) to predict upstream regulator(s) of *Egr1*. PAR4 [27], Elk3 (TCF subfamily) [26, 28], and PAR1 [27, 29] are an upstream candidate for *Egr1*. The default setting for data resources, confidential level, relation types, node types and mutation are shown. Tissue and cell lines used are endothelial cells (ECs), smooth muscle cells (SMCs) and cardiomyocytes (CMs), cardiovascular disease and connective tissue disorders are included in the analysis. **(B)** qPCR analysis of *Fbln4*, *Egr1*, *Elk3a*, *Elk3b*, *Elk3c*, *Elk3d*, *PAR1* and *PAR4* in P90 ascending aortas of CTRL and *SMKO* (pooled 3 aortas) mice. Bars are means ± SEM from the technical triplicates.

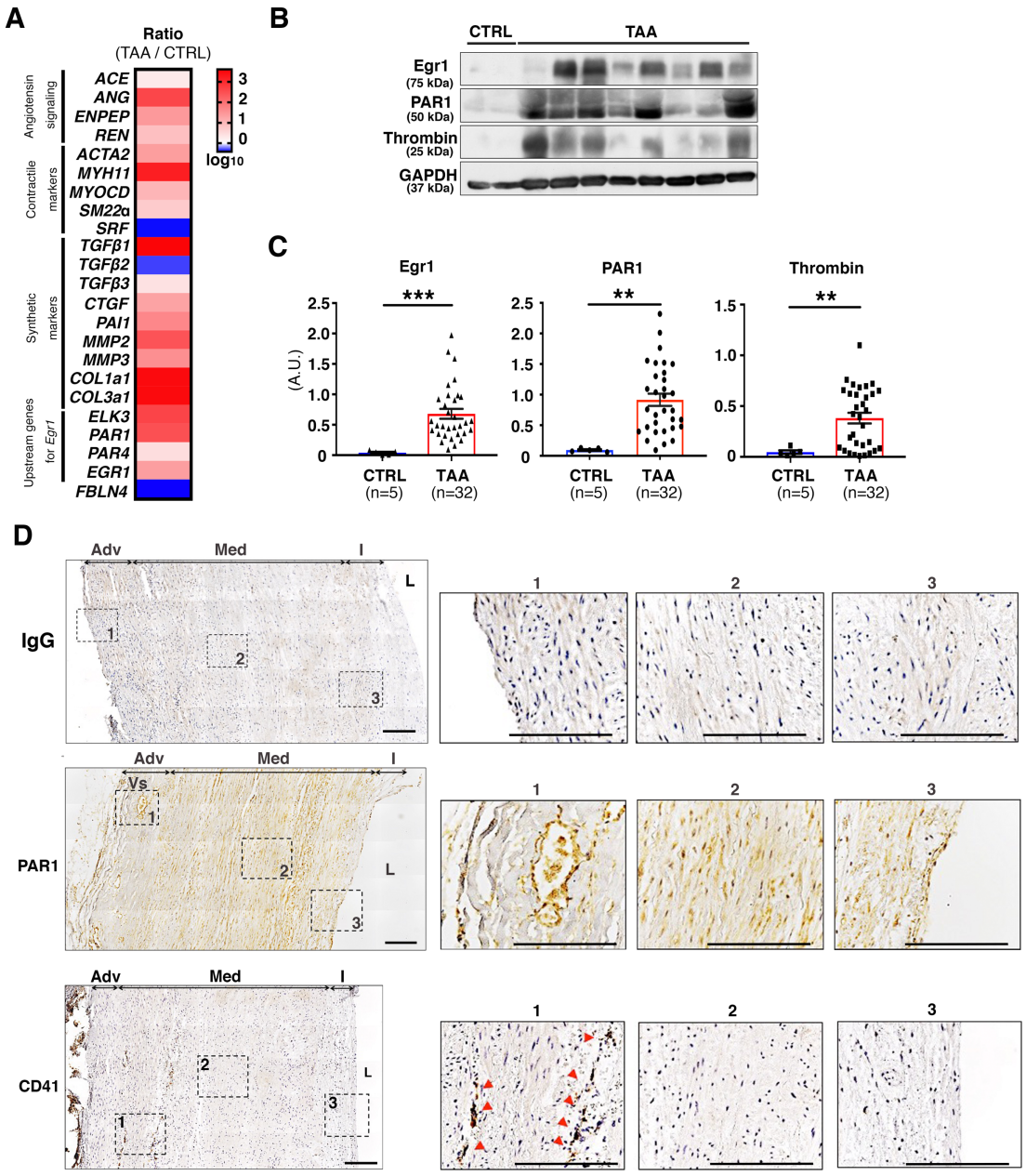

Figure 4. Egr1, PAR1 and its ligand, Thrombin are abundant in human TAA. (A) Heatmap showing the gene expression ratios (TAA/control) of angiotensin signaling, vascular SMC markers (contractile and synthetic) and upstream candidates for *Egr1*. Human aortic tissues from control (CTRL; pooled 2 aortas) and TAA (pooled 19 aortas) are used. **(B)** Representative Western blots of Egr1, PAR1, Thrombin (cleaved form: prethrombin and thrombin) and GAPDH in aortic tissues of CTRL (n=5, 1 or 2 aortas pooled per sample) and TAAs (n=32) from human patients. **(C)** Quantification graphs

of Egr1, PAR1 and Thrombin in B. Bars are means ± SEM. $^{**}P < 0.01$, $^{***}P < 0.001$, unpaired *t*-test for PAR1, Mann-Whitney test for Thrombin and Egr1. **(D)** Representative immunohistochemistry of cross sections of the human TAA (n=3) stained with mouse IgG as a negative control (top panel), anti-PAR1 (middle panel), and anti-CD41(bottom panel), counterstained with hematoxylin. I: Intima, Med: medial layer, Adv: Adventitia, Vs: Vaso vasorum, L: lumen. 1, 2, 3 are magnified images of TAAs showing adventitia, media, and intima, respectively. Arrow heads (red) indicate positive staining for CD41 (platelet glycoprotein IIb). Scale bars are 200 μm.

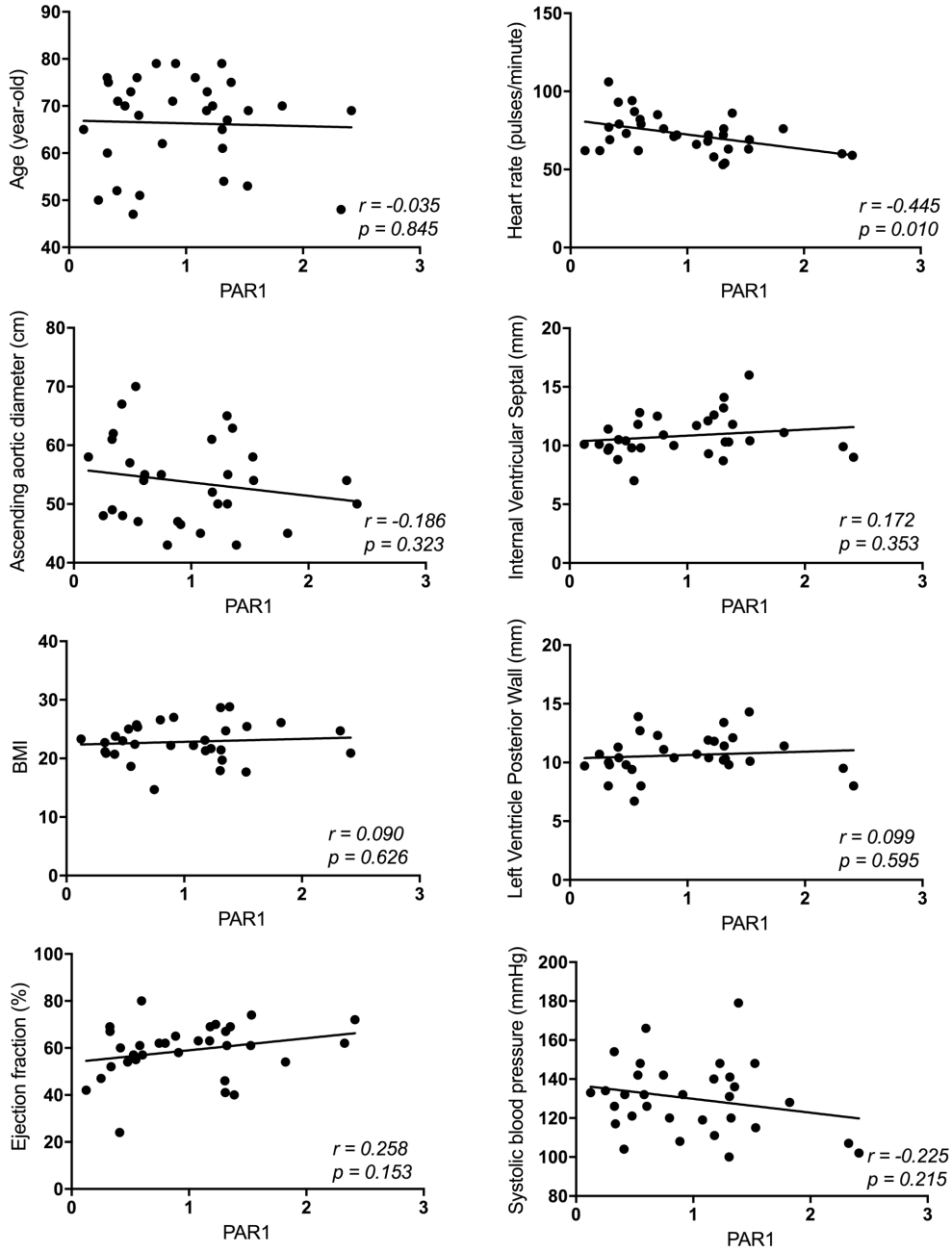

Figure 5. Correlation between PAR1 expression and clinical features in TAA patients. Each graph showing the correlation between PAR1 expression (showing in Fig. 4B) and clinical features, including age, aortic diameter, BMI, ejection fraction, heart rate, internal ventricular septal, left ventricle posterior wall, and systolic blood pressure. Pearson r shows correlation between PAR1 expression levels and each clinical feature, where +1 is total positive linear correlation, 0 is no linear correlation, and -1 is total negative correlation. Two-tailed *P* value are shown in graph.

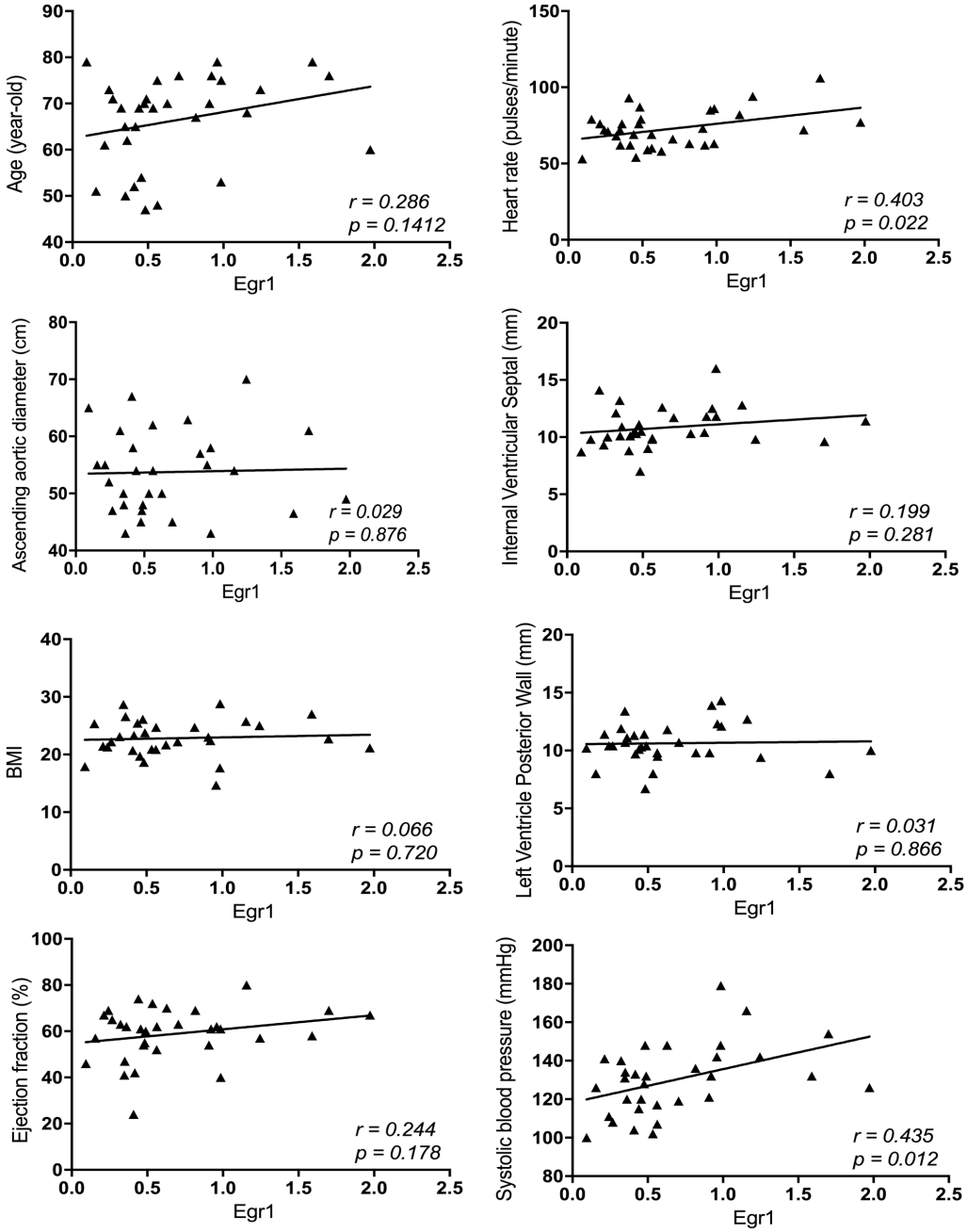

Figure 6. Correlation between Egr1 level and clinical features in TAA patients. Each graph showing the correlation between Egr1 level (showing in Fig. 4B) and clinical features, including age, aortic diameter, BMI, ejection fraction, heart rate, internal ventricular septal, left ventricle posterior wall, and systolic blood pressure. Pearson r shows correlation between Thrombin levels and each clinical feature, where +1 is total positive linear correlation, 0 is no linear correlation, and -1 is total negative correlation. Two-tailed *P* value are shown in graph.

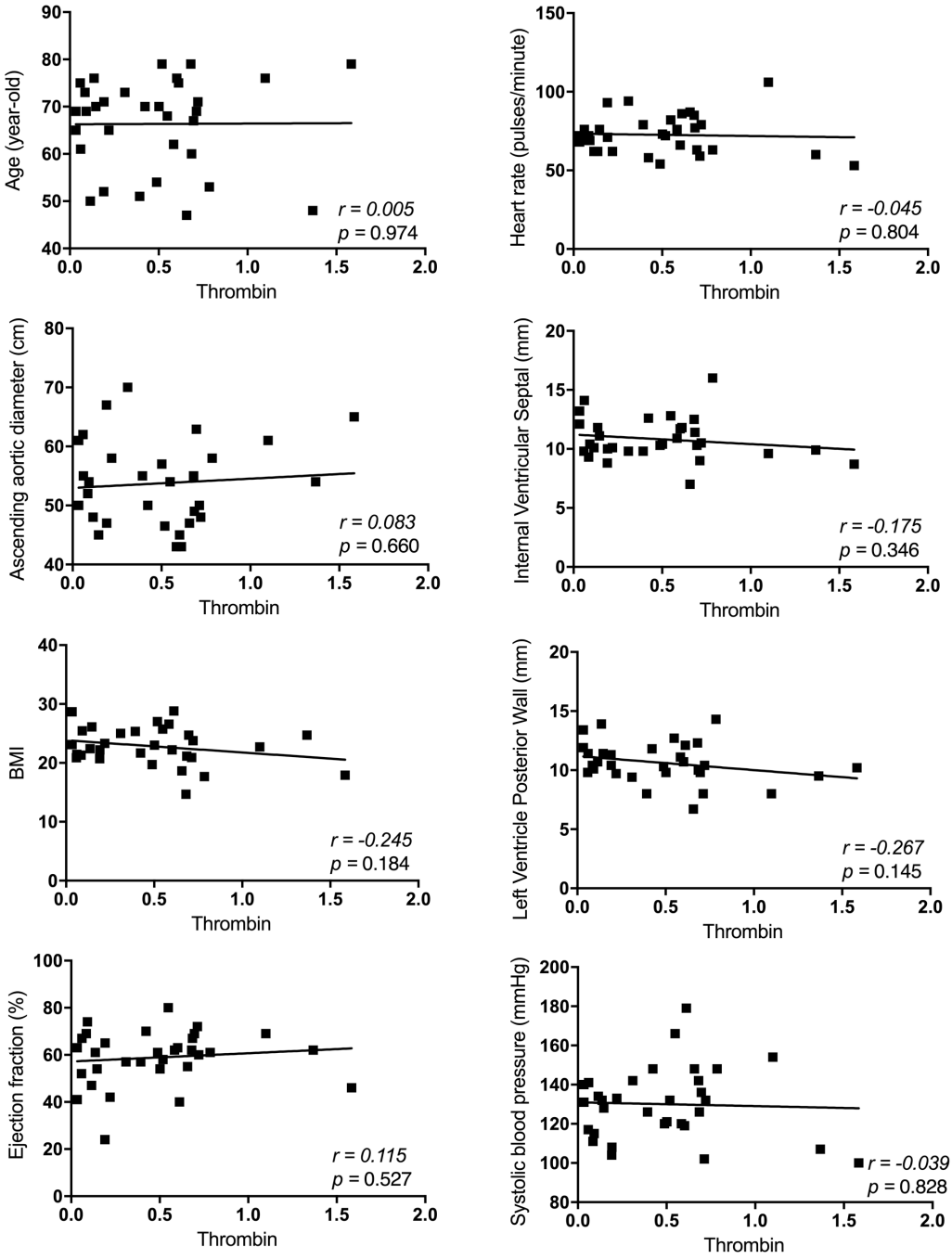

Figure 7. Correlation between thrombin expression and clinical features in TAA patients. Each graph showing the correlation between thrombin expression (showing in Fig. 4B) and clinical features, including age, aortic diameter, BMI, ejection fraction, heart rate, internal ventricular septal, left ventricle posterior wall, and systolic blood pressure. Pearson r shows correlation between Egr1 expression levels and each clinical feature, where +1 is total positive linear correlation, 0 is no linear correlation, and -1 is total negative correlation. Two-tailed *P* value are shown in graph.

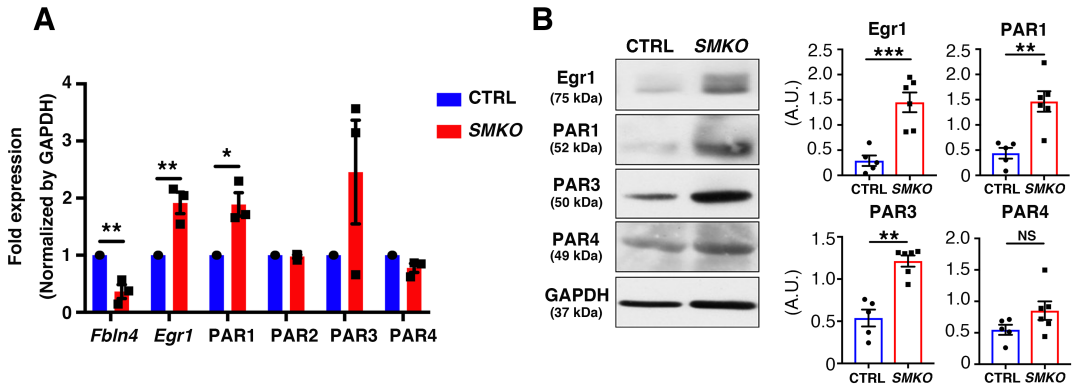

Figure 8. PAR1, Egr1 are highly activated in *SMKO* aortas at P1. (A) qPCR analysis of *Fbln4*, *Egr1*, *PAR1*, *PAR2*, *PAR3*, and *PAR4* in the entire aortas of postnatal day 1 (P1) CTRL and *SMKO* (n=3, 5 aortas pooled per sample) mice. Bars are means ± SEM. *$P < 0.05$. **$P < 0.01$, unpaired t-test. **(B)** Representative Western blots of Egr1, PAR1, PAR3, PAR4 and GAPDH in the entire aortas of P1 CTRL (n=5) and P1 *SMKO* (n=6). Quantification graphs are shown on the right. Bars are means ± SEM. **$P < 0.01$, ***$P < 0.001$, unpaired t-test for Egr1, PAR1 and PAR4, Mann-Whitney test for PAR3. NS: not significant.

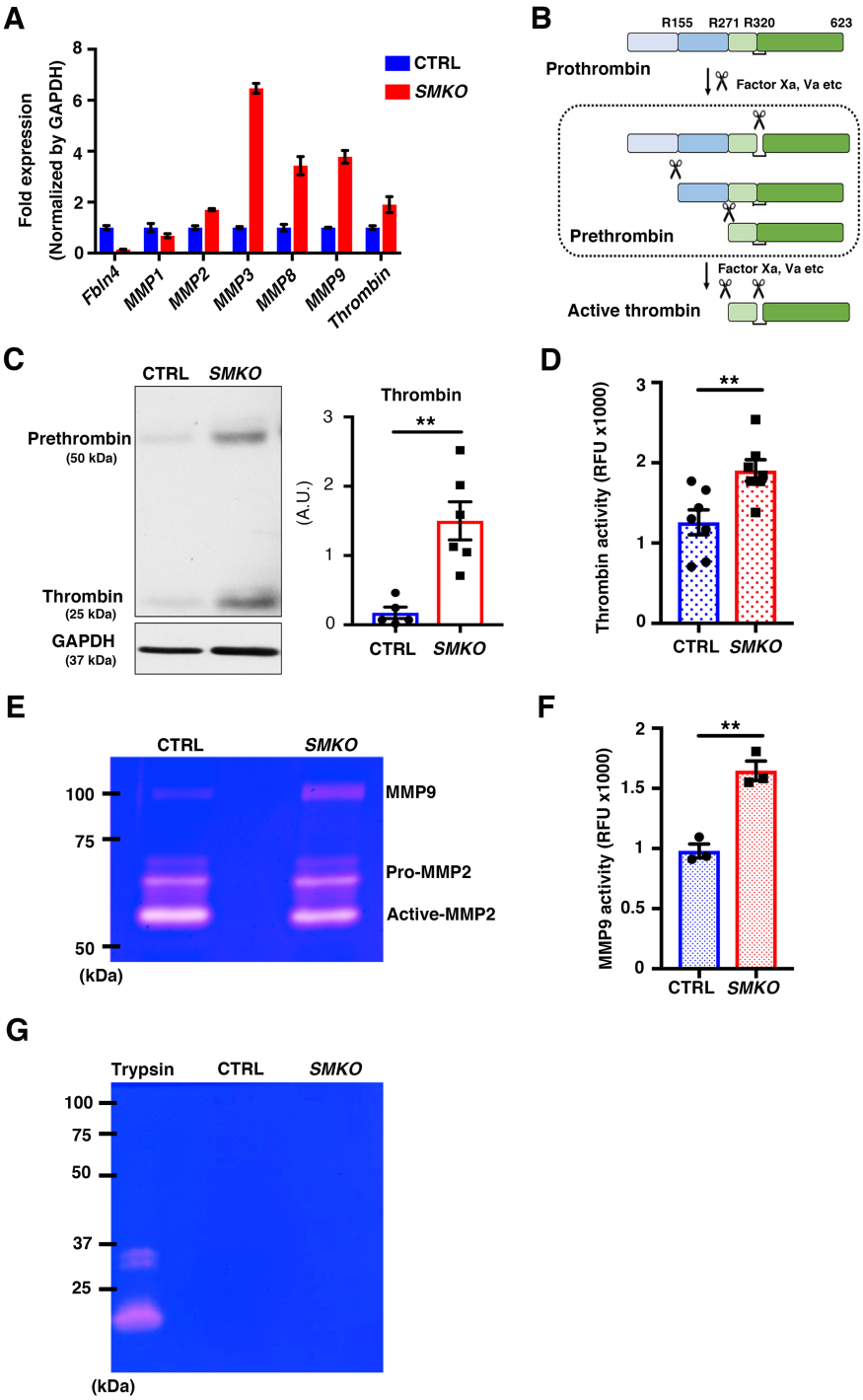
A
Fold expression (Normalized by GAPDH)
CTRL
SMKO
Fbln4
MMP1
MMP2
MMP3
MMP8
MMP9
Thrombin
B
R155 R271 R320 623
Prothrombin
Factor Xa, Va etc
Prethrombin
Factor Xa, Va etc
Active thrombin
C
CTRL SMKO
Prethrombin (50 kDa)
Thrombin (25 kDa)
GAPDH (37 kDa)
Thrombin
(A.U.)
**
CTRL SMKO
D
Thrombin activity (RFU x1000)
**
CTRL SMKO
E
CTRL SMKO
100
75
50
(kDa)
MMP9
Pro-MMP2
Active-MMP2
F
MMP9 activity (RFU x1000)
**
CTRL SMKO
G
Trypsin CTRL SMKO
100
75
50
37
25
(kDa)

Figure 9. PAR1 ligands, Thrombin and MMP9 are highly activated in *SMKO* aortas at P1.

(A) qPCR analysis of *Fbln4*, *MMP1*, *MMP2*, *MMP3*, *MMP8*, *MMP9* and *Thrombin* in P1 thoracic aortas of CTRL and *SMKO* mice. Bars are means ± SEM from the technical triplicates. **(B)** A schematic presentation of the conversion from prothrombin to active thrombin by proteolytic cleavage at R155, R271 and R320 by factor Xa and/or factor Va. **(C)** Representative Western blots of thrombin and GAPDH in the entire aortas of P1 CTRL (*n*=5) and P1 *SMKO* (*n*=6). Quantification graphs are shown on the right. Bars are means ± SEM. $^{**}P < 0.01$, unpaired *t*-test. **(D)** Thrombin activity assay using CTRL (*n*=7) and *SMKO* (*n*=7) entire aortas at P1. Bars are means ± SEM. $^{**}P < 0.01$, unpaired *t*-test. **(E)** Representative image of gelatin zymography of P1 entire aortas of CTRL (*n*=3, 3 aortas pooled per sample) and *SMKO* (*n*=3, 3 aortas pooled per sample). **(F)** MMP-9 activity assay using CTRL (*n*=3) and *SMKO* (*n*=3) entire aortas at P1. Bars are means ± SEM. $^{**}P < 0.01$, unpaired *t*-test. **(G)** Representative image of casein zymography of P1 entire aortas of CTRL (*n*=2, 3 aortas pooled per sample) and *SMKO* (*n*=2, 3 aortas pooled per sample). 0.1 g trypsin (20 kDa) is used for positive control in this experiment.

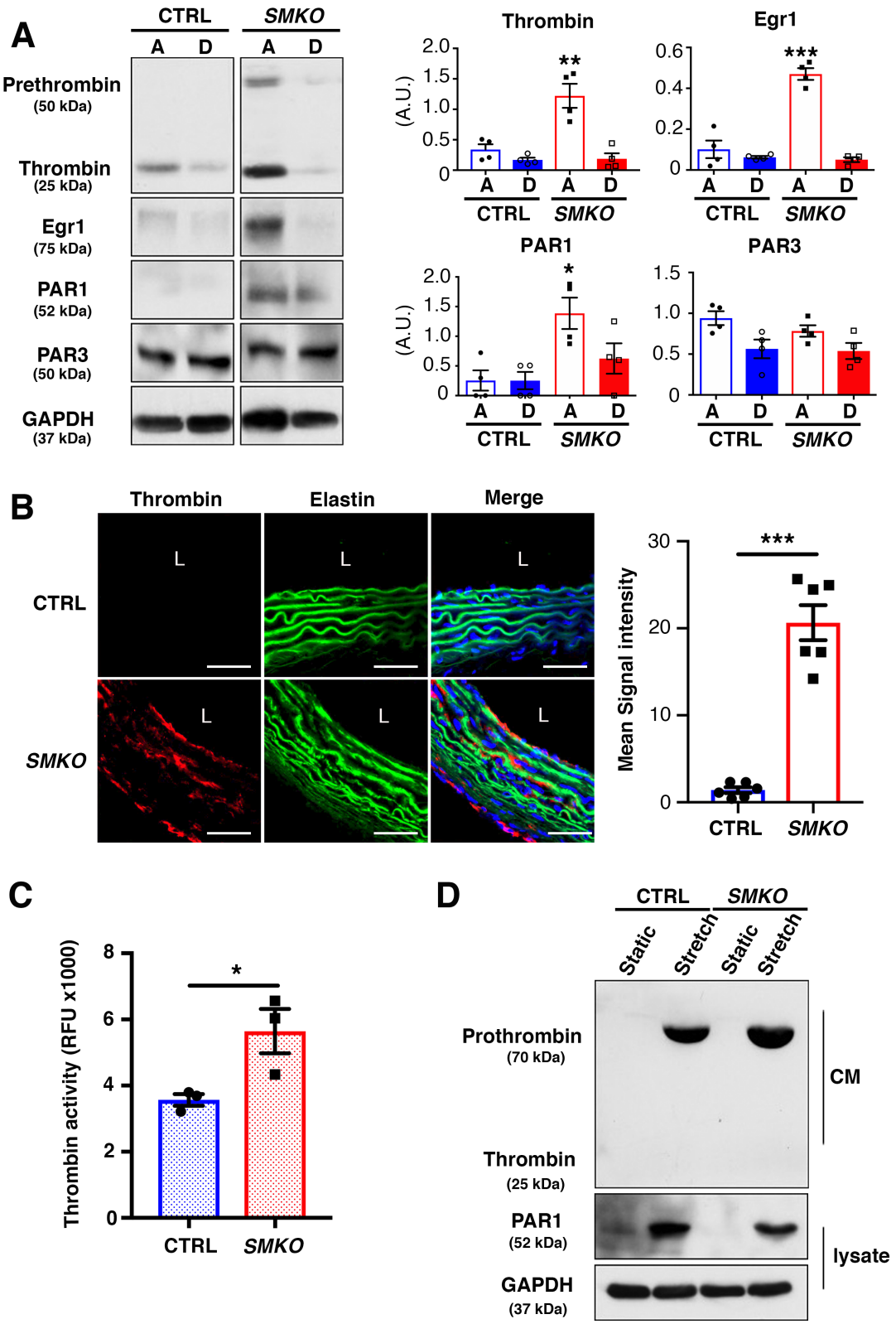
A
CTRL
SMKO
A D A D
Prethrombin
(50 kDa)
Thrombin
(25 kDa)
Egr1
(75 kDa)
PAR1
(52 kDa)
PAR3
(50 kDa)
GAPDH
(37 kDa)
Thrombin
Egr1
PAR1
PAR3
(A.U.)
**
***
*
CTRL
SMKO
B
Thrombin
Elastin
Merge
CTRL
SMKO
L
Mean Signal intensity
***
C
Thrombin activity (RFU x1000)
*
D
Static
Stretch
Prothrombin
(70 kDa)
Thrombin
(25 kDa)
PAR1
(52 kDa)
GAPDH
(37 kDa)
CM
lysate

Figure 10. PAR1 and thrombin are upregulated by mechanical stretch and expressed in SMCs of the aneurysm wall. (A) Representative Western blots of thrombin, Egr1, PAR1, PAR3 and GAPDH in CTRL (*n*=4) and *SMKO* (*n*=4) at P30 aortas from ascending (A) and descending (D) portions. Quantification graphs are shown on the right. **P* < 0.05, ***P* < 0.01, ****P* < 0.001, one-way ANOVA. Bars are means ± SEM. NS: not significant. **(B)** Cross sections of the ascending aortas from P30 CTRL (*n*=3) and *SMKO* (*n*=3) mice, immunostained with anti-Thrombin (red). DAPI (4',6-diamidino-2-phenylindole, blue) and elastic fibers (autofluorescence: green). Scale bars indicate 40 μm. Quantification graph show the mean signal intensity of thrombin per aortic area. Bars are means ± SEM. ****P* < 0.001, unpaired *t*-test. **(C)** Thrombin activity assay using CTRL (*n*=3) and *SMKO* (*n*=3) P30 ascending aortas. Bars are means ± SEM. **P* < 0.05, unpaired *t*-test. **(D)** Primary mouse SMCs isolated from CTRL or *SMKO* aortas were subjected to cyclic stretch (1.0 Hz; 20% strain) for 8h. After stretch, conditioned medium (CM) and cell lysates were harvested and performed Western blots. Representative Western blots show prothrombin from CM, and Egr1and PAR1 in cell lysates. *n*=2 per condition.

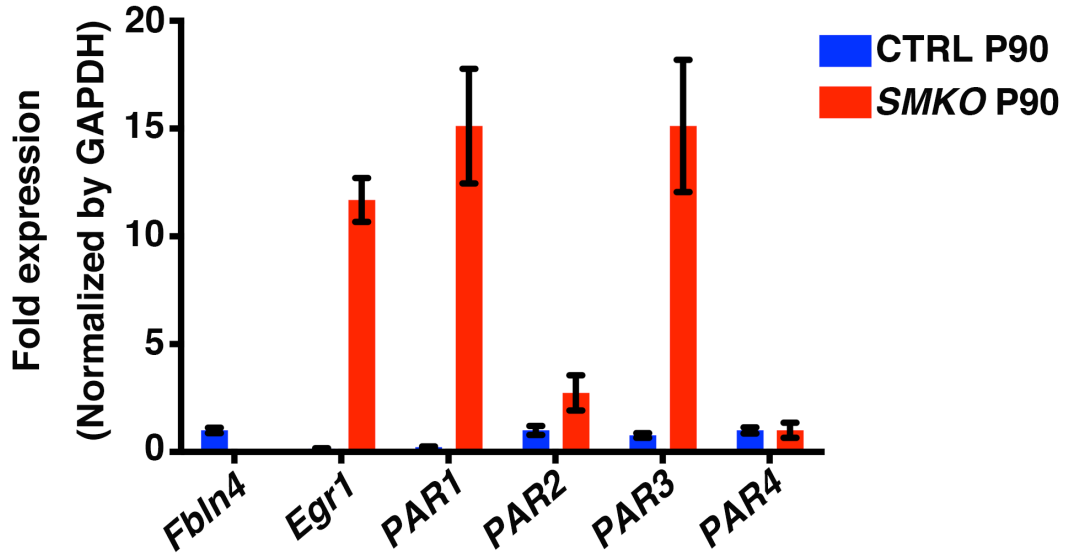

Figure 11. qPCR analysis of *SMKO* aortas after aneurysms are formed. qPCR analysis of *Fbln4*, *Egr1*, *PAR1*, *PAR2*, *PAR3*, and *PAR4* in P90 ascending aortas of CTRL and *SMKO* (pooled 3 aortas) mice. Bars are means ± SEM from the technical triplicates.

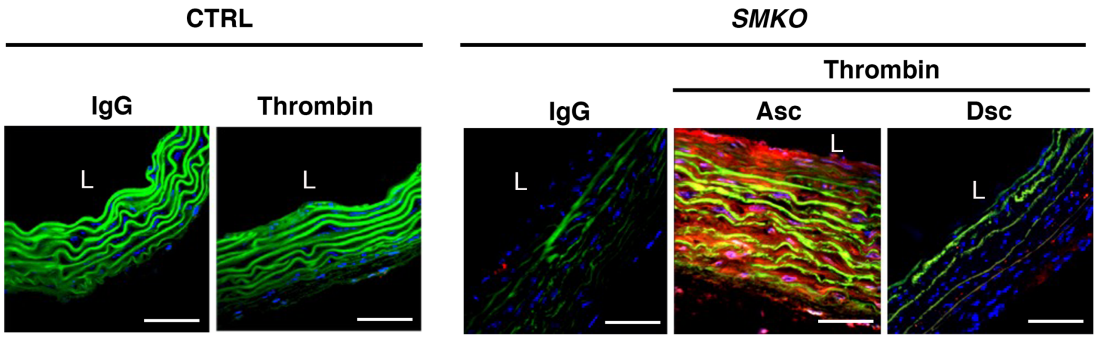

Figure 12. Thrombin is abundant in aneurysmal wall (related to Fig. 12B). Cross sections of the ascending aortas from P30 CTRL (*n*=3), ascending aortas and descending aortas from P30 *SMKO* (*n*=3, respectively), immunostained with anti-Thrombin (red), DAPI (blue) and elastic fibers (autofluorescence: green). Mouse IgG was used as a negative control. L: lumen. Scale bars indicate 40 μm.

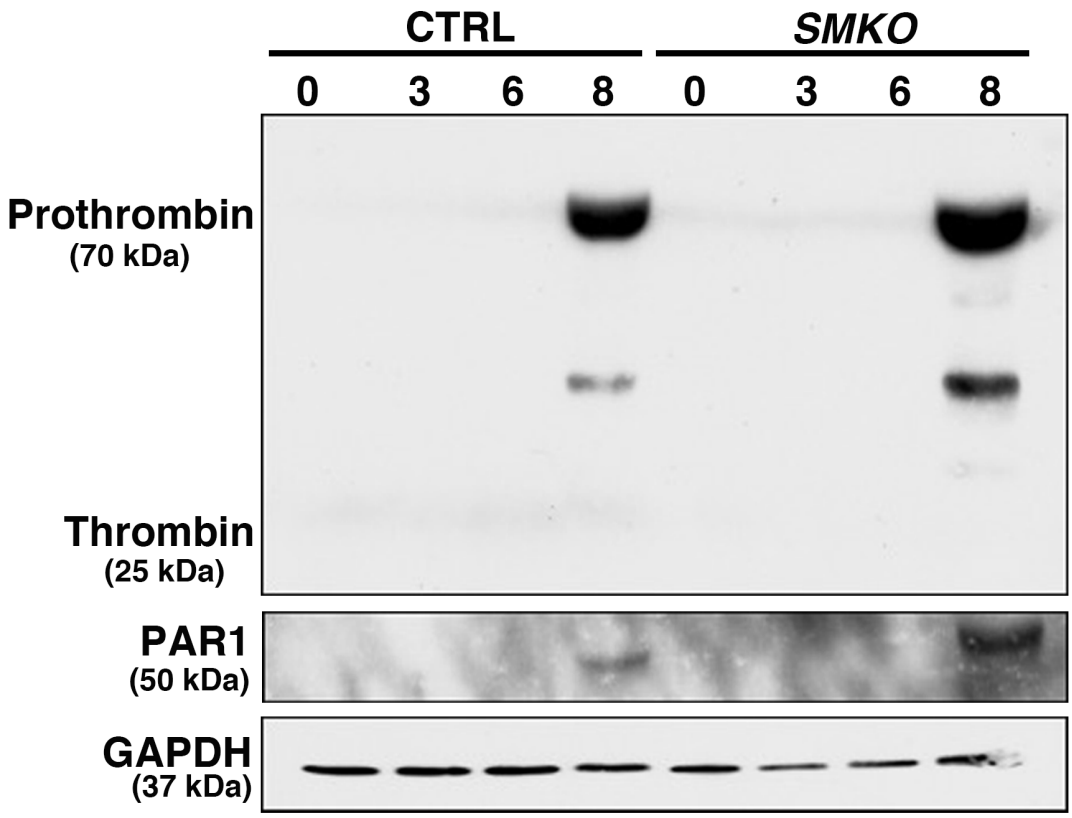

Figure 13. Cyclic stretch assay using primary mouse SMCs isolated from CTRL or *SMKO* aortas. (D) Primary mouse SMCs isolated from P30 CTRL or *SMKO* aortas were subjected to cyclic stretch (1.0 Hz; 20% strain) for 0, 3, 6 and 8h. After stretch, conditioned medium (CM) and cell lysates were harvested and performed Western blots.

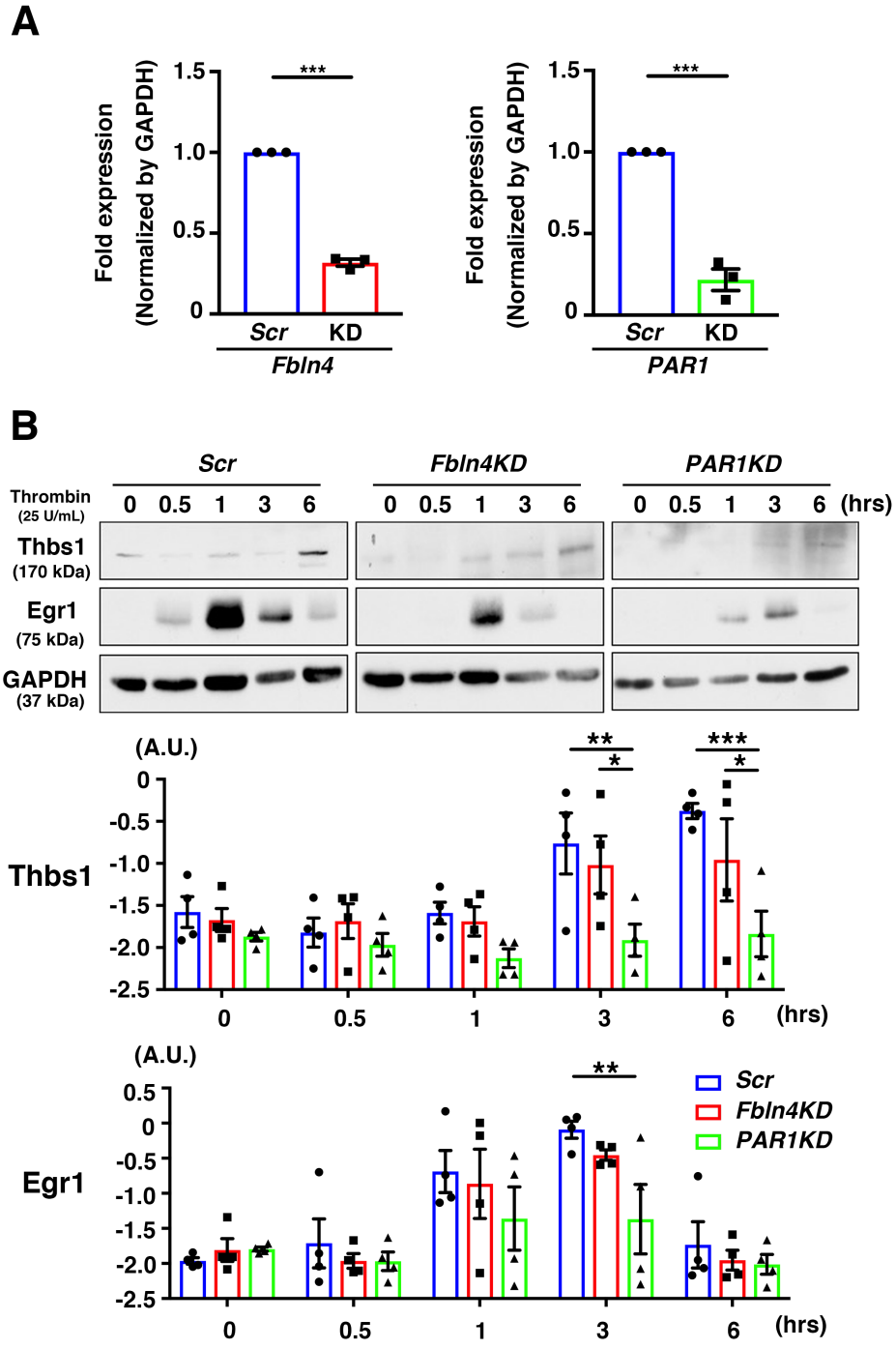

Figure 14. Thrombin-induced upregulation of Egr1 and Thbs1 is mediated by PAR1. (A) Quantitative polymerase chain reaction (qPCR) confirming the knockdown of *PAR1* and *Fbln4* by small interfering RNA (siRNA) in rat SMCs. Bars are means ± SEM. ***$P < 0.001$, unpaired *t*-test. **(B)** Scramble (Scr) or *PAR1* or *Fbln4* siRNA-treated rat SMCs were cultured in serum free media for 24 hours (hrs) and stimulated with or without thrombin (25 Unit/mL) for indicated time points. Representative

Western blots from quadruplicate experiments and quantification graphs with log-converted value of Thbs1/GAPDH and Egr1/GAPDH are shown on the bottom. Bars are means ± SEM. *P< 0.05, **P< 0.01, two-way ANOVA.

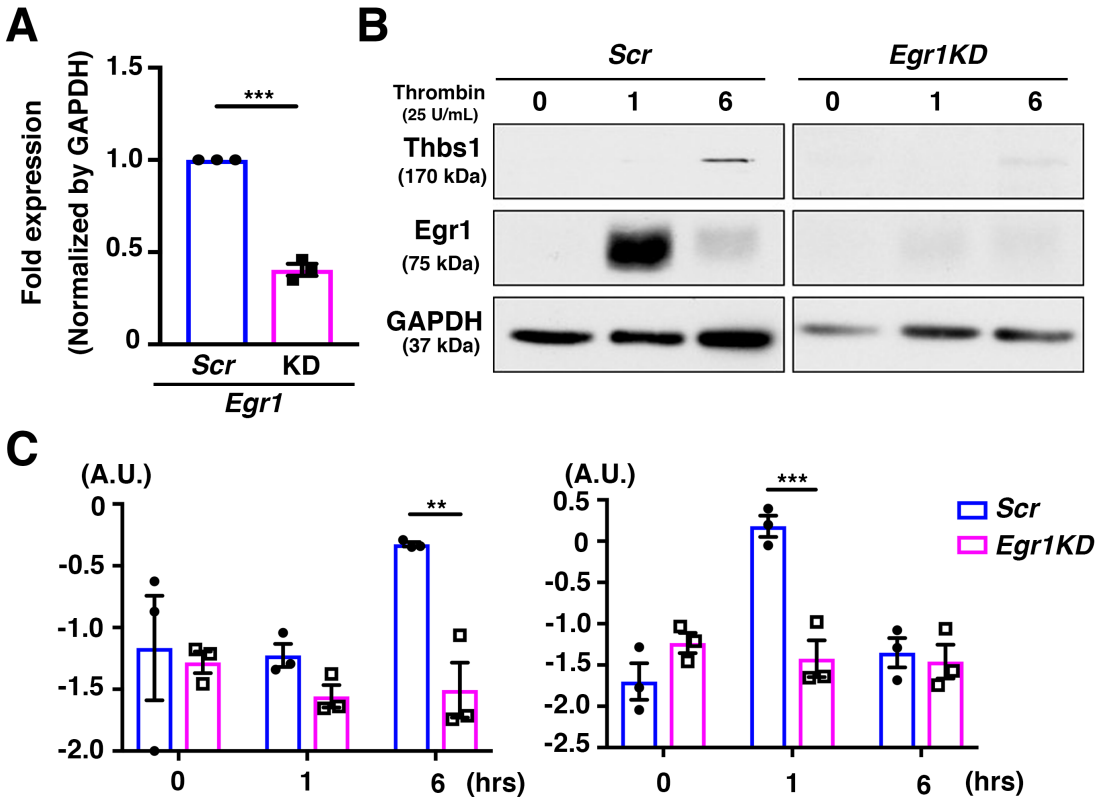

Figure 15. Thrombin treatment experiment between CTRL and *Egr1KD* rat SMCs. (A) qPCR confirming the knockdown of *Egr1* siRNA in rat SMCs. Bars are means ± SEM. ***$P < 0.001$, unpaired *t*-test. **(B)** Scr or *Egr1* siRNA-treated rat SMCs were cultured in serum free media for 24 hours (hrs) and stimulated with or without thrombin (25 Unit/mL) for indicated time points. Representative Western blots from triplicate experiments. **(C)** Quantification graphs showing log-converted value of Thbs1/GAPDH and Egr1/GAPDH. Bars are means ± SEM. **$P< 0.01$, ***$P< 0.001$, two-way ANOVA.

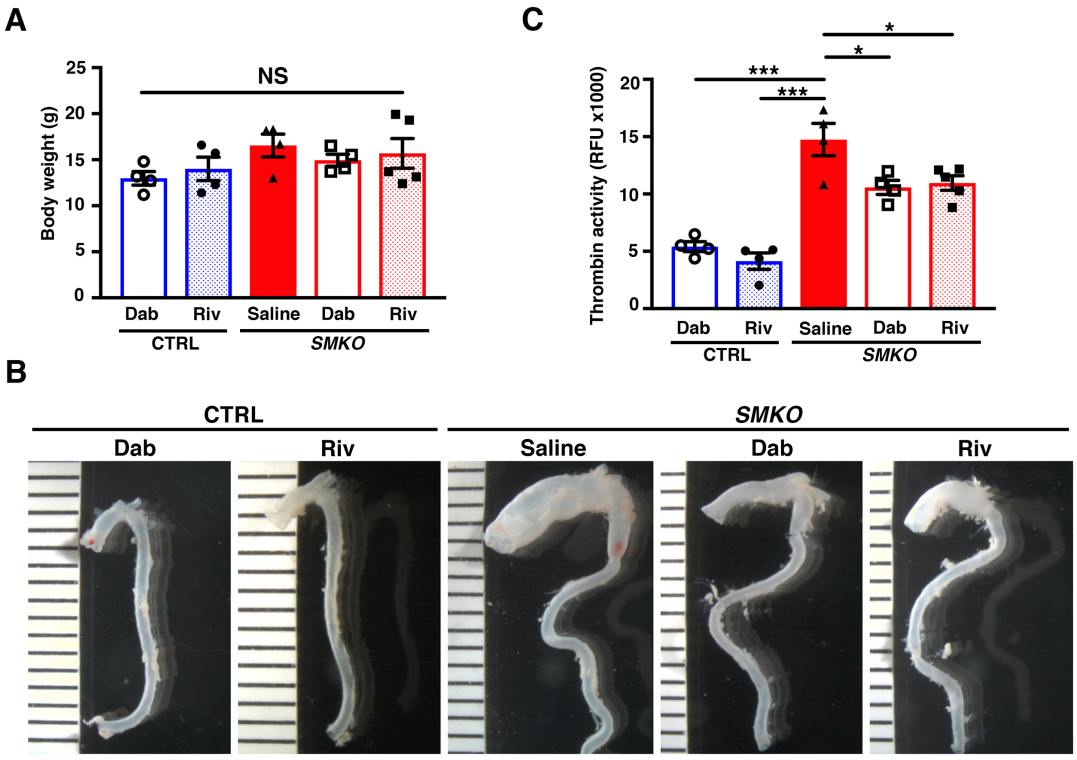

Figure 16. Pharmacological inhibition of thrombin and factor Xa in *SMKO*s (A) Comparison of body weight among Saline (vehicle)-, Dabigatran (Dab)-, or Rivaroxaban (Riv)- treated *SMKOs* at P30. Each point indicates a different animal. Bars are means ± SEM. one-way ANOVA. NS: not significant. **(B)** Representative gross photos of CTRL treated with Dab or Riv and *SMKO* treated with Saline, Dab or Riv at P30. Scale of bars is 1 mm. **(C)** Thrombin activity assay using ascending aortas of CTRL treated with Dab (n=4) or Riv (n=4) and *SMKO* treated with Saline (n=4), Dab (n=4) or Riv (n=5). Bars are means ± SEM. *$P < 0.05$, ***$P < 0.001$, one-way ANOVA.

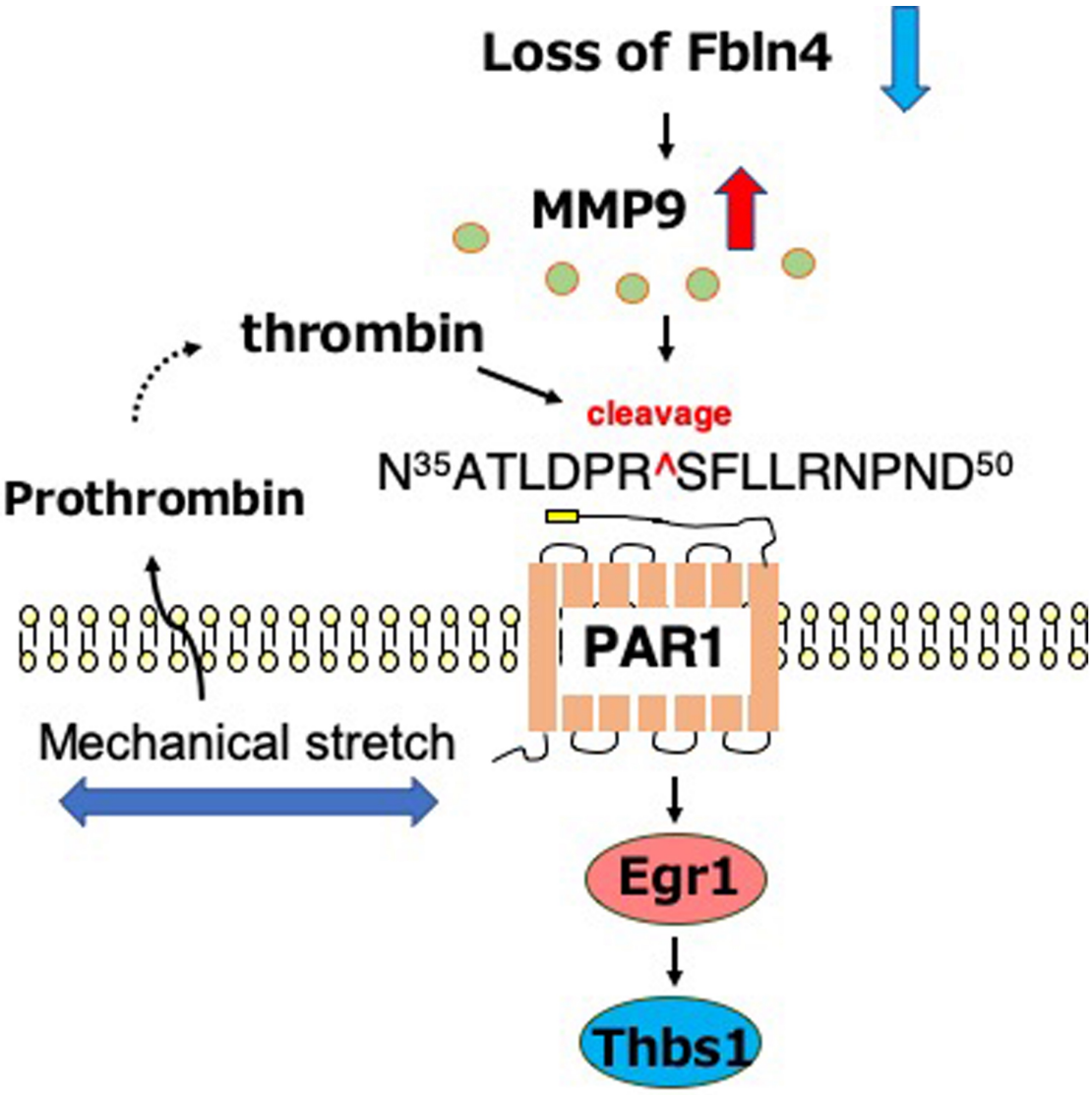

Figure 17. A model illustrating a potential mechanism of PAR1-Egr1 activation in the aneurysm wall. Absence of *Fbln4* in SMCs leads to an increase in MMP-9 activity, and simultaneously mechanical stretch induces PAR1 expression and secretion of prothrombin. Thrombin and MMP-9 mediates proteolytic activation of PAR1, leading to downstream signaling involving Egr1-Thbs1 and initiation of the aneurysm formation.